A Nonlinear Least Squares Framework for Periodic Grating Identification with a HOPS Implementation

BY

MATTHEW CHRISTOPHER KAPLAN
B.S., University of Texas, 2012
M.S., University of Illinois Chicago, 2014

THESIS
Submitted as partial fulfillment of the requirements
for the degree of Doctor of Philosophy in Mathematics
in the Graduate College of the
University of Illinois at Chicago, 2018

Chicago, Illinois

Defense Committee:
- Alexey Cheskidov
- David Nicholls, Chair and Advisor
- Christof Sparber
- Jan Verschelde
- Misun Min, Argonne National Laboratory

Acknowledgements

Thank you Dave for providing me invaluable academic guidance when most others would have advised me to be careful not to let the door hit me on my way out. Thank you Ramin for convincing me to stay. Thank you Erica for putting up with my nonsense. Thank you Camilla for being wonderful.

mk

Summary

This thesis focuses upon the scattering of time-harmonic plane waves by a periodic interface. In particular, we consider an inverse problem which involves reconstruction of the interface when provided with measured scattered field quantities along an artificially imposed "transparent" boundary layer close to the interface. Appealing to a High-Order Perturbation of Surfaces methodology coupled with a Nonlinear Least Squares framework, we numerically simulate the scattered field at the "transparent" boundary using the former and ultimately reconstruct the interface using the latter. We furnish numerical results which compare favorably to alternative methodologies employed to solve related inverse problems, and demonstrate the efficiency and accuracy of our numerical schemes.

Contents

List of Figures

CHAPTER 1

Mathematical Foundations

1. Introduction

1.1. Background. The scattering of linear electromagnetic waves by a layered structure is a central model in many problems of engineering interest. Our primary focus is on the interaction of visible and near-visible radiation with periodic structures on the micron or nanometer scales which are relevant for many applications in nanoplasmonics. We present a new identification algorithm for precisely providing this information built upon a Nonlinear Least Squares (NLS) framework and implemented with a High-Order Perturbation of Surfaces (HOPS) methodology which is orders of magnitude faster than volumetric solvers, and outperforms surface methods (such as Boundary Integrals) for the geometries under present consideration.

A standard structure [**93**] of particular interest involves a metallic diffraction grating which motivates us to consider a doubly layered configuration composed of a metal (e.g., gold or silver) overlaid with a dielectric (e.g., air or water) featuring a periodically corrugated interface. Assuming that the constituent materials are known, we further consider two important and related questions:

1. Given the shape of the interfaces, can one compute scattering quantities given incident radiation?

2. Having specified (several) incident waves and measured scattering returns, can one deduce information about the interface shape between the two layers?

Here we discuss both the "forward" and "inverse" problems, items 1 and 2 respectively, and propose a novel algorithm for the latter. Our method is based upon the method of Field Expansions of Bruno and Reitich ([**18**], [**19**], [**20**], [**21**], [**22**], [**23**], [**24**], [**25**]), a HOPS algorithm which is rapid, robust, and ideally suited to the scaling regime under consideration here.

1.2. Forward Problem. In the engineering literature there is a preponderance of volumetric approaches to these problems with a particular focus upon Finite Difference [**63**], Finite Element [**58**], Discontinuous Galerkin [**53**], Spectral Element [**34**], and Spectral [**42**], [**97**] methods. Clearly, such methods are disadvantaged with an unnecessarily large number of degrees of freedom for the piecewise homogeneous problem we consider here. Additionally, the correct application of outgoing wave conditions is an issue. This complication typically necessitates approximation such as the Perfectly Matched Layer [**6**], [**7**] or an exact, nonreflecting boundary condition [**57**], [**52**], [**60**], [**41**], [**79**], [**16**] which spoils the sparseness properties of the relevant linear systems.

Due to these factors, surface methods are an appealing choice as they are orders of magnitude quicker than volumetric approaches due to the greatly reduced number of unknowns required to resolve a computation. In addition, far-field boundary conditions are enforced exactly through the choice of the Green function. As such, these methods are a compelling alternative which are gaining favor with engineers. The most prevalent among these interfacial algorithms are Boundary Integral Equation (BIE) methods [**32**], [**96**], but these face difficulties as well. Most have been resolved in recent years through (i.) the use of sophisticated quadrature rules to deliver High-Order Spectral (HOS) accuracy; (ii.) the design of preconditioned iterative solvers with suitable acceleration [**43**]; (iii) new strategies to accelerate the convergence of the periodized Green function [**17**], [**13**] (or avoiding its periodization entirely [**10**], [**27**]); and (iv.) new approaches to deal with the Rayleigh singularities (widely known in the literature as "Wood's anomalies") [**4**], [**9**], [**26**]. Consequently, they are a tempting alternative for many problems of applied interest, however, they can be disadvantaged for the class of problems we consider as compared with the methods we advocate here due to the the dense, non-symmetric positive definite systems of linear equations that must be solved with each simulation.

In contrast, a HOPS methodology effectively addresses this concern. These algorithms have the advantageous properties of BIE formulations (e.g., surface formulation, reduced numbers of unknowns, and exactly outgoing solutions) while being immune to the criticism listed above: The scheme is built upon the flat-interface solution which is trivially solved in Fourier space by inverting a sparse operator at each wavenumber. We point out that the implied smallness assumption on the deformation can be dropped in light of the analytic continuation results in [**82**], [**47**] which demonstrate that the domain of analyticity contains a neighborhood of the entire real axis. Therefore, with appropriate numerical analytic continuation strategies (e.g., Pade approximation [**11**]) to access this region of analyticity, quite large and irregular perturbations can be simulated. We direct the interested reader to [**20**], [**22**], [**25**], [**81**], [**84**] for numerical demonstrations. There are many HOPS algorithms for the solution of partial differential equations posed on irregular domains, but they all originate in the low-order calculations of Rayleigh [**94**] and Rice [**95**]. The first high-order approaches were the Operator Expansions (OE) method of Milder [**66**], [**67**], [**72**], [**73**] and FE method of Bruno and

Reitich [**19**], [**20**], [**21**]. Each has been enhanced by various authors, but the most significant was the stabilization of these methods by Nicholls and Reitich with the Transformed Field Expansions (TFE) algorithm [**80**], [**81**], [**82**], [**83**], [**84**]. Beyond this, these HOPS schemes have been extended in a number of directions. For instance for bounded obstacle configurations [**24**], [**86**], [**40**], the full vector Maxwell equations [**23**], [**76**], [**90**], and multiply layered media [**49**], [**48**], [**50**]. For a rigorous numerical analysis please see [**87**].

1.3. Inverse Problem. The discussion thus far has been limited to the "forward problem" which is not our focus; our real goal is to address the "inverse problem." A vast amount of work has been conducted on this problem and one can consult any one of the following reference texts for more details [**30**], [**32**], [**62**], [**28**], [**29**]. The paper of X. Jiang and P. Li [**56**] gives a nice survey of previous results on this topic with specific application to the periodic two-dimensional periodic grating structures under consideration here. Their paper includes the following citations (included for the reader's convenience) on uniqueness and stability [**2**], [**8**], [**61**], [**45**], [**3**], and assorted computational approaches [**38**], [**39**], [**44**], [**5**], [**36**], [**1**], [**14**]. Of special note is the extensive line of work of P. Li and collaborators on inversion strategies based upon HOPS methods (in particular the TFE algorithm [**84**]). More specifically, techniques for phaseless data [**12**], [**100**] and nearfield measurements [**33**], [**15**].

Our inversion strategy is inspired by the work of Nicholls and M. Taber [**88**], [**89**] on the recovery of topography shape under a layer of an ideal fluid, and the discovery of sediment layer shapes from acoustic signals in a geoscience inversion strategy outlined by Nicholls and A. Malcolm [**68**], [**70**]. In each of these, rather explicit formulas for HOPS expansions of surface integral operators (Dirichlet-Neumann Operators) were used to identify relations involving the interface shape which could be iterated to produce a form which best explained the data observed. While we also use HOPS methods in this contribution, we do not rely heavily upon the specific forms of the terms in the expansions for our strategy. Instead, we adopt a rather general NLS framework [**59**], [**91**] where we define a particular residual to minimize in a least squares sense. To achieve this we appeal to the well known Gauss-Newton (GN) and Levenberg-Marquardt (LM) algorithms for iteratively minimizing this residual [**59**], [**91**], [**101**].

Before we fully discuss our contribution, we pause to present the relevant theoretical foundations our approach is built upon starting with two-dimensional scattering and the Helmholtz equation.

2. The Helmholtz Equation

2.1. Two-Dimensional Scattering. Consider a region S and let $\underline{\mathbf{E}}$ and $\underline{\mathbf{H}}$ denote the total electric and magnetic fields in S filled with a homogeneous material of constant permittivity ε, and zero charge density and current, respectively. In consideration of our particular scenario, we assume that the permeability of all materials μ is given by a constant μ_0 equal to the permeability of the vacuum. Next, consider a d-periodic grating structure $g(x)$ which separates S over its period into regions $S^{(u)}$ and $S^{(w)}$ filled with homogeneous materials of constant permittivities $\varepsilon^{(u)}$ and $\varepsilon^{(w)}$, respectively; in the event that the region $S^{(w)}$ is a perfect conductor, we need only consider a single permittivity, $\varepsilon^{(u)}$.

Now suppose we illuminate the grating $g(x)$ with time-harmonic plane-wave incidenct radiation:

(1a) $$\underline{\mathbf{E}}^i(x,z,t) = \mathbf{A}e^{i\alpha x - i\gamma z - i\omega t},$$

(1b) $$\underline{\mathbf{H}}^i(x,z,t) = \mathbf{B}e^{i\alpha x - i\gamma z - i\omega t}.$$

Where, for wavenumber k and angle of incidence θ, $\alpha = k\sin\theta$, and $\gamma = k\cos\theta$. Factoring out the $e^{-i\omega t}$ term, and under the assumptions above, both $\underline{\mathbf{E}}$ and $\underline{\mathbf{H}}$ in $S^{(u)}$ satisfy the time-harmonic Maxwell Equations

(2a) $$\nabla \times \underline{\mathbf{E}} = i\omega\mu_0\underline{\mathbf{H}},$$

(2b) $$\nabla \times \underline{\mathbf{H}} = i\omega\varepsilon\underline{\mathbf{E}},$$

(2c) $$\nabla \cdot \underline{\mathbf{E}} = 0,$$

(2d) $$\nabla \cdot \underline{\mathbf{H}} = 0.$$

Observe that by taking the curl of (2a) and substituting this into the left side of (2b) yields the Helmholtz equation

(3) $$\Delta\underline{\mathbf{E}} + k^2\underline{\mathbf{E}} = 0,$$

where $k^2 = \varepsilon\mu_0\omega^2$. A similar calculation shows that $\underline{\mathbf{H}}$ also satisfies (3).

For the case where $S^{(w)}$ is a perfect conductor, we see that the total field in $S^{(u)}$ can be decomposed into the diffracted and incident fields denoted by superscripts d and i, respectively

$$\underline{\mathbf{E}} = \underline{\mathbf{E}}^i + \underline{\mathbf{E}}^d, \tag{4a}$$

$$\underline{\mathbf{H}} = \underline{\mathbf{H}}^i + \underline{\mathbf{H}}^d, \tag{4b}$$

with boundary condition at the interface $g(x)$

$$\mathbf{n} \times \underline{\mathbf{E}} = 0, \tag{5a}$$

where $\mathbf{n}$ denotes the outward-pointing normal vector.

For the case when $S^{(w)}$ is filled with a homogeneous material, the total field decomposition given in (4) still applies to $\underline{\mathbf{E}}^{(u)}$ and $\underline{\mathbf{H}}^{(u)}$ while $\underline{\mathbf{E}}^{(w)}$ and $\underline{\mathbf{H}}^{(w)}$ in $S^{(w)}$ consists of scattered fields alone. These are coupled together with the boundary conditions at $g(x)$ given by

$$\mathbf{n} \times \left(\underline{\mathbf{E}}^{(u)} - \underline{\mathbf{E}}^{(w)}\right) = 0, \tag{6a}$$

$$\mathbf{n} \times \left(\underline{\mathbf{H}}^{(u)} - \underline{\mathbf{H}}^{(w)}\right) = 0, \tag{6b}$$

with $\mathbf{n}$ as above. Note that we employ the superscripts u and w in (6) to distinguish the total fields found in $S^{(u)}$ or $S^{(w)}$, respectively.

The d-periodicity of $g(x)$ implies that both $\underline{\mathbf{E}}$ and $\underline{\mathbf{H}}$ are quasi-periodic in x:

$$\underline{\mathbf{E}}(x + d, z) = e^{i\alpha d}\underline{\mathbf{E}}(x, z), \tag{7a}$$

$$\underline{\mathbf{H}}(x + d, z) = e^{i\alpha d}\underline{\mathbf{H}}(x, z), \tag{7b}$$

Thus, we are interested in quasi-periodic solutions to the Helmholtz equation with appropriate boundary conditions.

2.2. Boundary Conditions. To formulate appropriate boundary conditions along the grating interface $g(x)$, we assume g is invariant in the y direction and the incident radiation is transversely aligned with the grating yielding boundary conditions for the Transverse Electric (TE) and Transverse Magnetic (TM) polarization cases.

2.2.1. *Transverse Electric.* For a Perfectly Conducting interface at $z = g(x)$ we have

$$u^d = -u^i, \tag{8a}$$

while for the interface between two dielectrics at $z = g(x)$ we have

$$u^d - w^d = -u^i, \tag{9a}$$

$$\partial_{\mathbf{n}} u^d - \partial_{\mathbf{n}} w^d = -\partial_{\mathbf{n}} u^i, \tag{9b}$$

where u and w are the quasi-periodic y components of the electric field in $S^{(u)}$ and $S^{(v)}$, respectively.

2.2.2. *Transverse Magnetic.* For a Perfect Conducting interface at $z = g(x)$ we have

$$\partial_{\mathbf{n}} u^d = -\partial_{\mathbf{n}} u^i, \tag{10a}$$

while for the interface between two dielectrics at $z = g(x)$ we have

$$u^d - w^d = -u^i, \tag{11a}$$

$$\partial_{\mathbf{n}} u^d - \tau^2 \partial_{\mathbf{n}} w^d = -\partial_{\mathbf{n}} u^i, \tag{11b}$$

where u and w are the quasi-periodic y components of the magnetic field in $S^{(u)}$ and $S^{(v)}$, respectively, and

$$\tau^2 = \frac{\varepsilon_u}{\varepsilon_w}.$$

To formulate appropriate boundary conditions at infinity, we must consider bounded and outward propagating solutions of the quasi-periodic Helmholtz equation; we shall see that such solutions satisfy a so-called outgoing wave condition (OWC).

2.3. Rayleigh Expansions. We are interested in solving the following boundary value problem

$$\Delta u + k^2 u = 0, \tag{12a}$$

$$u(x, g(x)) = -u^i(x, g(x)), \tag{12b}$$

$$u(x + d, z) = e^{i\alpha d} u(x, z), \tag{12c}$$

where solutions satisfy an OWC. It is a straightforward calculation to show that for $z > \|g\|_\infty$ the solution to (13) in $S^{(u)}$ is given by

$$u(x, z) = \sum_{p \in \mathbb{Z}} A_p e^{i\alpha_p x + i\gamma_p z} + B_p e^{i\alpha_p x - i\gamma_p z}, \tag{13}$$

where

$$\alpha_p := \alpha + \frac{2\pi}{d} p, \qquad \gamma_p := \begin{cases} \sqrt{k^2 - \alpha_p^2} & \text{if } p \in U \\ i\sqrt{\alpha_p^2 - k^2} & \text{if } p \notin U, \end{cases} \tag{14}$$

with

$$U = \{p \in \mathbb{Z} \mid \alpha_p^2 < k^2\}. \tag{15}$$

To enforce the requirements that (14) is indeed outward propagating and bounded, we demand that $B_p \equiv 0$, otherwise (14) is inward propagating for $p \in U$, and unbounded for $p \notin U$. Thus we have appropriate solutions to (13) given by

$$u(x, z) = \sum_{p \in \mathbb{Z}} A_p e^{i\alpha_p x + i\gamma_p z}. \tag{16}$$

We note that by a similar rationale we have, for $z < \|g\|_\infty$, the solution to (13) in $S^{(w)}$ is given by

$$w(x, z) = \sum_{p \in \mathbb{Z}} A_p e^{i\alpha_p x - i\gamma_p z}. \tag{17}$$

We next wish to formulate our boundary value problem in a way that enables efficient numerical simulation. This leads us to decompose the domain $S^{(u)}$ by inserting an artificial boundary at $z = a$ and define

$$S_a^{(u)} = \{z : g(x) < z < a\}. \tag{18}$$

This yields the following boundary value problem

$$\Delta u + k^2 u = 0, \qquad u \in S_a^{(u)}, \tag{19a}$$

$$u(x, g(x)) = -u^i(x, g(x)), \qquad z = g, \tag{19b}$$

$$u(x + d, z) = e^{i\alpha d} u(x, z), \tag{19c}$$

$$\Delta v + k^2 v = 0, \qquad z > a, \tag{19d}$$

$$u = v, \qquad z = a, \tag{19e}$$

$$\partial_z u = \partial_z v, \qquad z = a, \tag{19f}$$

$$v(x + d, z) = e^{i\alpha d} v(x, z), \tag{19g}$$

with the OWC satisfied by v. We note that solutions to (19d) are as in (18):

$$v(x, z) = \sum_{p \in \mathbb{Z}} \widetilde{A}_p e^{i\alpha_p x + i\gamma_p z}, \tag{20}$$

and by (19e) we have

$$v(x, z) = \sum_{p \in \mathbb{Z}} a_p e^{i\alpha_p x + i\gamma_p (z-a)}. \tag{21}$$

The condition in (19f) enables us to define a Dirichlet-Neumann Operator(DNO)

$$T : v(x, a) \to (\partial_z v)(x, a), \tag{22}$$

and reformulate this condition as

$$(\partial_z u) - (\partial_z v) = (\partial_z u) - T[u] = 0. \tag{23}$$

This yields an equivalent formulation of (19):

$$\Delta u + k^2 u = 0, \qquad u \in S_a^{(u)}, \tag{24a}$$

$$u(x, g(x)) = -u^i(x, g(x)), \qquad z = g, \tag{24b}$$

$$u(x + d, z) = e^{i\alpha d} u(x, z), \tag{24c}$$

$$(\partial_z u) - T[u] = 0, \qquad z = a. \tag{24d}$$

Since we wish to numerically simulate the coefficients to the solution of (24), we appeal to the principle of energy conservation to indicate convergence of our approximations.

2.4. Conservation of Energy. We note that [**92**] defines the p^{th} efficiency as

$$e_p = \frac{\gamma_p}{\gamma}|A_p|^2, \qquad p \in U, \tag{25}$$

and proceeds to show that in the case that $S^{(w)}$ is a perfect conductor,

$$\sum_{p \in U^{(u)}} e_p^{(u)} = 1. \tag{26}$$

A similar condition holds in the case of both $S^{(u)}$ and $S^{(w)}$ filled with homogeneous dielectric materials:

$$\sum_{p \in U^{(u)}} e_p^{(u)} + \tau^2 \sum_{p \in U^{(w)}} e_p^{(w)} = 1. \tag{27}$$

Thus we may define an "energy defect"

$$\delta := 1 - \sum_{p \in U^{(u)}} e_p^{(u)}, \tag{28a}$$

$$\delta := 1 - \sum_{p \in U^{(u)}} e_p^{(u)} - \tau^2 \sum_{p \in U^{(w)}} e_p^{(w)}, \tag{28b}$$

which furnishes an appropriate diagnostic of convergence for our numerical methods solving the "forward problem" for the perfectly electric conducting (PEC) (29a) and for both the PEC and transverse electric (TE) cases (29b).

2.5. An Additional Verification Method. In addition to appealing to an energy conservation principle to ensure the convergence of our forward solver, we note that [**33**] formulates a reconstruction formula which employed the Transformed Field Expansions (TFE) method to approximate a periodic interface from a measured data field from some constant height above the grating as an additional method of validating our forward solver. The formula is given by

$$\hat{g}_p = -\frac{i}{2k}(\hat{u}_{a,p} - \hat{u}_{a,0})e^{-i\gamma_p a}, \tag{29}$$

where $\hat{g}_p$ and $\hat{u}_{a,p}$ are the p^{th} Fourier coefficient of the grating and the far-field approximation at $z = a$, respectively; and,

$$\hat{u}_{a,0,p} = \begin{cases} e^{-ika} - e^{-ika} & p = 0 \\ 0 & p \neq 0. \end{cases} \tag{30}$$

We now discuss the High-Order Perturbation of Surfaces(HOPS) methods of Bruno and Reitich ([**18**], [**19**], [**20**], [**21**], [**22**], [**23**], [**24**], [**25**]) to approximate solutions to (24).

3. High-Order Perturbation of Surfaces

3.1. The Method of Field Expansions. We begin by noting that in the case that the interface $g \equiv 0$, the solution to (24) is given by

$$u(x,z) = \sum_{p \in \mathbb{Z}} \hat{u}_{a,p} e^{i\alpha_p x + \gamma_p z}. \tag{31}$$

Now suppose the interface $g(x)$ is not identically zero, and is a perturbation of a sufficiently smooth function f

$$g(x) = \varepsilon f(x), \quad \varepsilon \ll 1. \tag{32}$$

It was demonstrated by [**18**] that if f is analytic, then the field u depends analytically on ε. The regularity of f can be weakened, with C^2, $C^{1,\alpha}$, or even Lipschitz also working (for a rigorous proof in the case of C^2 profiles see [**80**], [**84**], while Lipschitz interfaces are considered in [**46**]). We point out that the smallness assumption on ε can be removed via analytic continuation [**82**], [**47**] which was numerically implemented using Padé summation [**20**], [**81**], [**84**]. This enables us to write

$$u(x,z) = u(x,z,\varepsilon) = \sum_{n=0}^{\infty} u_n(x,z)\varepsilon^n, \tag{33}$$

a convergent Taylor series. We now follow the approach taken by Nicholls and Reitich ([**80**], [**81**], [**82**], [**83**], [**84**]) in deriving Field Expansion (FE) recursions. Substitution of (31) into (24), differentiation with respect to ε n times, and setting ε to zero results in the following boundary value problem for each of the u_n:

$$\Delta u_n + k^2 u_n = 0, \qquad u \in S_a^{(u)}, \tag{34a}$$

$$u_n(x,0) = Q_n, \qquad z = 0, \tag{34b}$$

$$u_n(x+d,z) = e^{i\alpha d} u_n(x,z), \tag{34c}$$

$$(\partial_z u_n) - T[u_n] = 0, \qquad z = a, \tag{34d}$$

where

$$Q_n := -\frac{f(x)^n}{n!}(-i\gamma)^n e^{i\alpha x} - \sum_{m=0}^{n-1} \frac{f(x)^{(n-m)}}{(n-m)!} \partial_z^{n-m} u_m(x,0). \tag{35}$$

This last quantity arises from the fact that

$$\sum_{n=0}^{\infty} v_n(x,\varepsilon f)\varepsilon^n = \sum_{n=0}^{\infty} \left(\sum_{m=0}^{\infty} \frac{f(x)^m}{m!} \partial_z^m u_m(x,0)\varepsilon^m \right) \varepsilon^n = \sum_{n=0}^{\infty} \sum_{m=0}^{n} \frac{f(x)^{(n-m)}}{(n-m)!} \partial_z^{n-m} u_m(x,0)\varepsilon^n.$$

We note that order $n = 0$ corresponds to the $g \equiv 0$ case. Appealing to the rationale used above we may write the solution to (32) as

$$u_n(x,z) = \sum_{p\in\mathbb{Z}} a_{n,p} e^{i\alpha_p x + i\gamma_p z}. \tag{36}$$

The boundary condition (32b) yields

$$e^{i\gamma_p \varepsilon f} = \sum_{n=0}^{\infty} \frac{f(x)^n}{n!} (i\gamma_p)^n \varepsilon^n, \tag{37}$$

so equating at $O(\varepsilon^n)$ we have

$$a_{n,p} = \hat{\zeta}_{n,p} - \sum_{m=0}^{n-1} \sum_{r\in\mathbb{Z}} \hat{F}_{n-m,p-r} (i\gamma_r)^{n-m} a_{m,r}, \tag{38}$$

where

$$F_n(x) = \sum_{p\in\mathbb{Z}} \hat{F}_{n,p} e^{ipx}, \tag{39}$$

and

$$F_n(x) := \frac{f(x)^n}{n!}, \tag{40}$$

and

$$\zeta_n(x) = -F_n(-i\gamma)^n e^{i\alpha x}. \tag{41}$$

We may use (36) to recover the coefficients of the solution for all $z > \|g\|_\infty$ in terms of the series in (31):

$$v(x,z,\varepsilon) = \sum_{n=0}^{\infty} v_n(x,z)\varepsilon^n = \sum_{n=0}^{\infty}\sum_{p\in\mathbb{Z}} a_{n,p} e^{i\alpha_p x + i\gamma_p z}\varepsilon^n. \tag{42}$$

Thus we see that the method of FE for electromagnetic scattering of waves by a periodic grating enables one to substitute approximations of the Fourier coefficients $\{a_{n,p}\}$ of the solution for (32) into (40) to evaluate the field in a given region.

3.2. Dirichlet-Neumann Operator. In electromagnetic simulations the current is given by exterior surface normal derivative which we may approximate numerically by appealing to the method of FE. Recall the Dirichlet data from (24b) is given by

$$u(x, g(x)) = -u^i(x, g(x)),$$

and define the exterior Neumann data as

$$\nu(x) := [-\mathbf{n}\cdot\nabla u](x,g(x)) = [-\partial_z u + (\partial_x g)\partial_x u](x, g(x)), \tag{43}$$

where $\mathbf{n} := (-\partial_x g, 1)^T$. We define a second DNO

$$G(g) : u(x, g(x)) \to \nu, \tag{44}$$

which is both more useful in practice and more difficult to compute given that it involves a physical boundary instead of an artificial one as described previously. Using our previous work, computation of this operator may be done via FE.

For $g \equiv 0$ we first recall that

$$u(x,z) = \sum_{p\in\mathbb{Z}} \hat{u}_{0,p} e^{i\alpha_p x + i\gamma_p z},$$

so computation of $G(0)$ is easy:

$$G(0) = -\partial_z u(x, 0) = \sum_{p\in\mathbb{Z}} \hat{u}_{0,p}(-i\gamma_p)e^{i\alpha_p x}.$$

When $g \not\equiv 0$, we again adopt a perturbative approach, taking $g(x) = \varepsilon f(x)$, and note that the Neumann data depends analytically on ε which allows us to write

$$\nu(x,\varepsilon) = \sum_{n=0}^{\infty} \nu_n(x)\varepsilon^n.$$

Upon substitution of this series into (41) yields

$$\nu(x,\varepsilon) = \sum_{n=0}^{\infty} [-\partial_z u_n + (\partial_x \varepsilon f)\partial_x u_n](x, \varepsilon f(x))\varepsilon^n,$$

which gives us at $O(\varepsilon^n)$

$$\nu_n = -\sum_{m=0}^{n} F_{n-m}\partial_z^{n+1-m} u_m(x,0) + \sum_{m=0}^{n-1} (\partial_x f) F_{n-m-1}\partial_z^{n-1-m} u_m(x,0). \tag{45}$$

Ultimately we find

$$\hat{\nu}_n = -\sum_{m=0}^{n}\sum_{r\in\mathbb{Z}} \hat{F}_{n-m,p-r}(i\gamma_r)^{n+1-m} a_{m,r} + \sum_{m=0}^{n-1}\sum_{r\in\mathbb{Z}} \hat{F}'_{n-1-m,p-r}(i\alpha_r)(i\gamma_r)^{n+1-m} a_{m,r},$$

where

$$F'_m(x) := (\partial_x f)F_m(x).$$

3.3. Three Dimensions. We end this section by generalizing our preceding discussion to three-dimensions in a natural way. We first consider the domain

$$S^{(u)} := \{z > g(x,y)\},$$

where g is a bi-periodic grating

$$g(x+d_1, y+d_2) = g(x,y).$$

The bi-periodicity of g induces (α,β) - quasiperiodicity

$$u(x+d_1, y+d_2) = e^{i\alpha d_1} e^{i\beta d_2} u(x,y,z),$$

and we can enforce the OWC by writing solutions as

$$u(x,y,z) = \sum_{p\in\mathbb{Z}}\sum_{q\in\mathbb{Z}} a_{p,q} e^{i\alpha_p x + i\beta_q y + i\gamma_{p,q} z}, \tag{46}$$

where

$$\alpha_p := \alpha + \frac{2\pi}{d_1}p, \tag{47a}$$

$$\beta_q := \beta + \frac{2\pi}{d_2}q, \tag{47b}$$

$$\gamma_{p,q} := \begin{cases} \sqrt{k^2 - \alpha_p^2 - \beta_q^2}, & (p,q) \in U \\ i\sqrt{\alpha_p^2 + \beta_q^2 - k^2}, & (p,q) \notin U, \end{cases} \tag{47c}$$

with

$$U = \{(p,q) \in \mathbb{Z}^2 : \alpha_p^2 + \beta_q^2 < k^2\}. \tag{48}$$

Which leads to the boundary value problem

$$\Delta u + k^2 u = 0, \qquad u \in S_a^{(u)}, \tag{49a}$$

$$u(x,y,g(x)) = -u^i(x,y,g(x,y)), \qquad z = g, \tag{49b}$$

$$u(x+d_1, y+d_2, z) = e^{i\alpha d_1} e^{i\beta d_2} u(x,y,z), \tag{49c}$$

$$(\partial_z u) - T[u] = 0, \qquad z = a, \tag{49d}$$

where

$$S_{g,a} := \{g(x,y) < z < a\}, \tag{50}$$

denotes the domain with transparent boundary, and

$$T[u] = \sum_{p\in\mathbb{Z}} \sum_{q\in\mathbb{Z}} (i\gamma_{p,q}) \hat{u}_{p,q} e^{i\alpha_p x + i\beta_q y}, \tag{51}$$

denotes the DNO, and u^i is incident radiation.

Beginning again with the assumption that

$$g(x,y) = \varepsilon f(x,y), \quad \varepsilon \ll 1$$

for a sufficiently smooth f, we again write

$$u(x,y,z,\varepsilon) = \sum_{n=0}^{\infty} v_n(x,y,z)\varepsilon^n, \tag{52}$$

and upon substitution into (49) leads to a system for every perturbation order n with corresponding solution given by

$$u_n(x,y,z) = \sum_{p\in\mathbb{Z}}\sum_{q\in\mathbb{Z}} a_{n,p,q} e^{i\alpha_p x + i\beta_q y + i\gamma_{p,q} z}. \tag{53}$$

Adopting a slightly different approach to the one developed in the two dimensional case, we consider

$$a_n(x,y) = \sum_{p\in\mathbb{Z}}\sum_{q\in\mathbb{Z}} a_{n,p,q} e^{i\alpha_p x + i\beta_q y}, \tag{54a}$$

$$a(x,y) = \sum_{p\in\mathbb{Z}}\sum_{q\in\mathbb{Z}} a_n(x,y)\varepsilon^n. \tag{54b}$$

and notice that

$$u_n(x,y,0) = a_n(x,y), \tag{55a}$$

$$u(x,y,0) = a(x,y), \tag{55b}$$

This enables one to to motivate our physical intuition: The function $a(x,y)$ is the "zero-trace" of the field u, while the functions $a_n(x,y)$ represent the n^{th} order Taylor corrections of $a(x,y)$ in an ε expansion with $g(x,y) = \varepsilon f(x,y)$. Keeping (53) in mind, we see that the $a_n(x,y)$ yield (α,β) quasiperiodic solutions for the Helmholtz equation that satisfy OWC. However, we must ensure that the Dirichlet boundary condition (49b) is also satisfied. This motivates us to define a Dirichlet operator

$$D(g) := a(x,y) = v(x,y,0) \to v(x,y,g(x,y)), \tag{56}$$

which maps the field's "zero-trace" to its "boundary-trace" value. Note that this operator is linear in a, but nonlinear in g.

Assuming that f is sufficiently smooth we may expand this in a Taylor series in ε

$$D(g) = D(\varepsilon f) = \sum_{n=0}^{\infty} D_n(f)\varepsilon^n, \tag{57}$$

and recall that

$$u(x,y,g(x,y)) = u(x,y,\varepsilon) = \sum_{n=0}^{\infty} u_n(x,y)\varepsilon^n. \tag{58}$$

Next, we see that since

$$D(\varepsilon f)[u(x,y,0)] = u(x,y,\varepsilon f), \tag{59}$$

then we have

$$\left(\sum_{n=0}^{\infty} D_n(f)\varepsilon^n\right)[e^{i\alpha_p x + i\beta_q y}] = e^{i\alpha_p x + i\beta_q y} e^{i\gamma_{p,q}\varepsilon f}, \tag{60}$$

and note that the rightmost term can be expressed as

$$e^{i\gamma_{p,q}\varepsilon f} = \sum_{n=0}^{\infty} (i\gamma_{p,q})^n F_n \varepsilon^n. \tag{61}$$

So we see that

$$D_0 e^{i\alpha_p x + i\beta_q y} = e^{i\alpha_p x + i\beta_q y}, \tag{62}$$

hence,

$$D_0 = I. \tag{63}$$

Now we consider

$$u_p(x,y,z) = e^{i\alpha_p x + i\beta_p y + i\gamma_p z}, \tag{64}$$

and substitute into the definition of D which yields

$$D_g(u_p(x,y,0)) = u_p(x,y,g(x,y)). \tag{65}$$

Again we take $g(x,y) = \varepsilon f(x,y)$ and expand this equation as Taylor series giving us

$$\left(\sum_{n=0}^{\infty} D_n(f)\varepsilon^n\right)(e^{i\alpha_p x + i\beta_p y}) = \sum_{n=0}^{\infty} F_n(x,y)(i\gamma_{p,q})^n e^{i\alpha_p x + i\beta_p y}\varepsilon^n, \tag{66}$$

from which immediately follows

$$D_n(f) = F_n(x,y)(i\gamma_D)^n. \tag{67}$$

we may similarly define N by

$$N : u(x,y,0) \to \partial_N u(x,y,g), \tag{68}$$

as

$$N = \left[-\partial_z u + \partial_x g \partial_x u + \partial_y g \partial_y u\right]_{z=g}. \tag{69}$$

It can be shown that

$$N = N(\varepsilon f) = \sum_{n=0}^{\infty} N_n(f)\varepsilon^n. \tag{70}$$

Again we consider

$$u_p(x,y,x) = e^{i\alpha_p x + i\beta_q y + i\gamma_{p,q} z}, \tag{71}$$

and note that

$$N(\varepsilon f) u_p(x,y,0) = \left[-\partial_z u + \varepsilon \partial_x f \partial_x u + \varepsilon \partial_y f \partial_y u\right]_{z=\varepsilon f}. \tag{72}$$

So we see that

$$\left(\sum_{n=0}^{\infty} N_n(f)\varepsilon^n\right)(e^{i\alpha_p x + i\beta_p y}) = A + B + C, \tag{73}$$

where

$$A = -i\gamma_{p,q} \sum_{n=0}^{\infty} F_n(x,y)(i\gamma_{p,q})^n e^{i\alpha_p x + i\beta_p y}\varepsilon^n, \tag{74a}$$

$$B = \varepsilon \partial_x f (i\alpha_p) \sum_{n=0}^{\infty} F_n(x,y)(i\gamma_{p,q})^n e^{i\alpha_p x + i\beta_p y}\varepsilon^n, \tag{74b}$$

$$C = \varepsilon \partial_y f (i\beta_q) \sum_{n=0}^{\infty} F_n(x,y)(i\gamma_{p,q})^n e^{i\alpha_p x + i\beta_p y}\varepsilon^n, \tag{74c}$$

$$N_n = -F_n(i\gamma_{p,q})^{n+1} + \partial_x f F_{n-1}(i\gamma_{p,q})^{n-1} + \partial_y f F_{n-1}(i\gamma_{p,q})^{n-1}. \tag{74d}$$

Using the preceding calculations we may define a DNO

$$GDa = Na, \tag{75}$$

which implies

$$GD = N, \tag{76}$$

from which it follows

$$G = ND^{-1}. \tag{77}$$

So we see that

$$\left(\sum_{n=0}^{\infty} G_n \varepsilon^n\right)\left(\sum_{m=0}^{\infty} D_m \varepsilon^m\right) = \left(\sum_{n=0}^{\infty} N_n \varepsilon^n\right), \tag{78}$$

and its easy to see that

$$G_0 D_0 = N_0, \tag{79a}$$

$$D_0 = I, \tag{79b}$$

$$G_0 = i\gamma_D, \tag{79c}$$

$$N_0 = i\gamma_D, \tag{79d}$$

$$G_n D_0 = N_n - \sum_{m=0}^{n-1} G_{0m} Dn - m, \tag{79e}$$

$$G_{0n} = N_n - \sum_{m=0}^{n-1} G_m D_{n-m}. \tag{79f}$$

The following section concludes this chapter which features a discussion of methods of the iterative optimization of nonlinear functions.

4. Nonlinear Least Squares

Recall that the goal of an unconstrained optimization problem is to determine a local minimizer x^* of a real-valued function f such that for $\delta \ll 1$, $f(x^*) \leq f(x)$ for all $x \in B_\delta(x^*)$ a ball of radius δ

centered at x^*. More succinctly: we seek to determine

$$\arg\min_x f(x). \tag{80}$$

Consider the nonlinear system of equations

$$R(x) = 0, \tag{81}$$

where $R(x) = (r_1(x), ..., r_M(x))^T$ is the residual. We specifically wish to identify the minimum of the objective function typically associated with NLS problems given by

$$f(x) = \frac{1}{2}\sum_{n=0}^{M} \|r_n(x)\|_2^2 = \frac{1}{2}R(x)^T R(x). \tag{82}$$

At a local minimizer x^* of f one may distinguish between the *zero residual problem* if $f(x^*) = 0$; the *small residual problem* if $f(x^*) \ll 1$; and the *large residual problem* for all other values of $f(x^*)$. We note that at x^* optimality implies $R'(x^*)^T R(x^*) = 0$.

We define the Jacobian R' of R as

$$(R'(x))_{ij} = \partial_{x_j} r_i,\ 1 \le i \le M, 1 \le j \le N, \tag{83}$$

and it is easy to see that

$$\nabla f = R'(x)^T R(x). \tag{84}$$

Additionally, the $N \times N$ Hessian is given as

$$\nabla^2 f(x) = R'(x)^T R'(x) + \sum_{i=1}^{N} r_i(x)^T \nabla^2 r_i(x). \tag{85}$$

Newton's Method for finding a zero of ∇f, which leads to a critical point of f which we hope is minimizer of f takes an initial guess x_0 and uses a correction v_k to update the current iterate x_k and reads

$$x_{k+1} = x_k + v_k, \tag{86}$$

where v_k solves

$$\nabla^2 f(x_k) v_k = -\nabla f(x_k). \tag{87}$$

By dropping terms in the Hessian, we are led to the GN method because near a minimizer the second derivatve of R is likely to be small.

4.1. Gauss-Newton Method. We note that since

$$\sum_{i=1}^{N} r_i(x)^T \nabla^2 r_i(x) = 0 \tag{88}$$

for zero residual problems, it is reasonable to assume that (53) is small for small residual problems which motivates us to drop this term, and eliminates the need to compute the second derivative. This yields the correction term v_k for GN:

$$-(\nabla^2 f(x_k))^{-1} \nabla f(x_k) \approx v_k = -(R'(x_k)^T R'(x_k))^{-1} R'(x_k)^T R(x_k), \tag{89}$$

and a GN iterate is given by

$$x_{k+1} = x_k + v_k. \tag{90}$$

Note that this assumes $R'(x_k)^T R'(x_k)$ is nonsingular. In the event that $R'(x_k)^T R'(x_k)$ is singular, one may appeal to the Moore-Penrose pseudoinverse $A^\dagger$ of a matrix A, which is defined in terms of the singular-value decomposition(SVD) of $A = U\Sigma V^T$:

$$A^\dagger = V \Sigma^\dagger U^T, \tag{91}$$

where U and V are orthonormal matrices with dimensions $M \times N$ and $N \times N$, respectively, and $\Sigma = \text{diag}(\sigma_1, ..., \sigma_N)$ is an $N \times N$ matrix, where for all $i \in \{1, ..., N\}$, σ_i is the i^{th} singular value. The columns of U and V are the left and right singular vectors of A, and we lastly note that

$$\Sigma^\dagger = \text{diag}(\sigma_1^\dagger, ..., \sigma_N^\dagger), \tag{92}$$

where

$$\sigma_i^\dagger = \begin{cases} \sigma_i^{-1} & \sigma_i \neq 0 \\ 0 & \sigma_i = 0. \end{cases}$$

We note that if A is nonsingular and square then $A^\dagger = A^{-1}$, and when A has full column rank

$$A^\dagger = (A^T A)^{-1} A^T, \tag{93}$$

which enables us to write $R'(x)^\dagger = -(R'(x_k)^T R'(x_k))^{-1} R'(x_k)^T$ which yields the GN correction term

$$v_k = -R'(x_k)^\dagger R(x_k). \tag{94}$$

It is shown in [**59**] that GN is particularly well-suited for overdetermined small residual problems with initial guesses close to local minima, but can be adjusted for both large residual NLS problems and initial guesses far from the root. Additionally, for the case of an underdetermined problem one may appeal to (56) at the expense of uniqueness.

4.1.1. *Steepest Descent.* We recall that the direction of steepest descent from x of a function f is in the direction of $-\nabla f(x)$. Motivated by this idea, we may update an iterate $x_{k+1} = x_k + v_k$ as in (55) where the correction term v_k is given by

$$v_k = -C\nabla f(x_k),$$

and the constant C is the stepsize. With this in mind, we see that the direction of steepest descent for (48) is

$$-\nabla f(x) = -R'(x)^T R(x).$$

In particular, the GN direction at x is given by (53), provided R' has full column rank. In this case we then see that

$$-(R'(x)^T R(x))^T (R'(x)^T R'(x))^{-1} R'(x)^T R(x) < 0,$$

which implies that the GN direction is a descent direction. In the event that $R'(x)^T R'(x)$ is singular, an adjustment can be made to ensure that updates to the current iterate are indeed in the direction of descent. This idea leads us to the LM method.

4.2. Levenberg-Marquardt. The LM method corrects for the case when $R'(x)^T R'(x)$ is singular by adding a reguarization parameter $\lambda > 0$ yielding the correction v_k given by

$$v_k = -(R'(x_k)^T R'(x_k) + \lambda_k I)^{-1} R'(x_k)^T R(x_k). \tag{95}$$

We see that the addition of the regularization parameter ensures that the $-(R'(x_k)^T R'(x_k) + \lambda_k I)^{-1}$ term from the correction v_k associated to the LM method is positive definite. We note that for small

λ this method resembles GN, while for large λ this method more closely behaves like a steepest descent algorithm. Thus one can think of LM as a combination of both GN and steepest descent depending upon the choice of λ which motivates how we decide to update the LM parameter.

4.2.1. *Updating the Levenberg-Marquardt Parameter.* For the objective function given by (48) we define

$$Ared_k = \|R(x_k)\|_2^2 - \|R(x_k + v_k)\|_2^2 \tag{96a}$$

$$Pred_k = \|R(x_k)\|_2^2 - \|R(x_k) + R'(x_k)v_k)\|_2^2, \tag{96b}$$

as the actual and predicted reductions of the objective function, respectively. By considering their ratio

$$r_k = \frac{Ared_k}{Pred_k},$$

a typical LM update of an iterate is performed by taking

$$x_{k+1} = \begin{cases} x_k + v_k, & \text{if } r_k \geq p_0, \\ x_k, & \text{if } r_k < p_0, \end{cases}$$

for constant p_0, and by taking

$$\lambda_{k+1} = \begin{cases} c_0\lambda_k, & \text{if } r_k < p_1, \\ \lambda_k, & \text{if } p_1 \leq r_k \leq p_2, \\ c_1\lambda_k, & \text{if } r_k > p_2, \end{cases}$$

for constants $0 < p_0 < p_1 < p_2 < 1$, and $0 < c_1 < 1 < c_0$.

A recent method of updating the LM parameter found in [**101**] sets

$$\lambda_k = \mu_k \|R(x_k)\|_2, \tag{97}$$

and updates μ_k by taking either

$$\mu_{k+1} = \begin{cases} c_0\mu_k, & \text{if } \|R'^T(x_k)R(x_k)\|_2 < \dfrac{p_1}{\mu_k}, \\ \mu_k, & \text{if } \dfrac{p_1}{\mu_k} \leq \|R'^T(x_k)R(x_k)\|_2 \leq \dfrac{p_2}{\mu_k}, \\ \max\{c_1\mu_k, m\}, & \text{if } \|R'^T(x_k)R(x_k)\|_2 > \dfrac{p_2}{\mu_k}, \end{cases} \tag{98}$$

where $0 < m \ll 1$, or

$$\mu_{k+1} = c_0\mu_k. \tag{99}$$

Lastly to update the iterate we take either

$$x_{k+1} = x_k + v_k, \text{ if } r_k \geq p_0, \tag{100}$$

and compute μ_{k+1} by (63), or we take

$$x_{k+1} = x_k, \text{ if } r_k > p_0, \tag{101}$$

and compute μ_{k+1} by (64).

CHAPTER 2

Implementation and Numerical Results

We are now poised to present the main result given that we have provided the requisite background mathematical material.

1. Governing Equations

Consider Figure 1 which displays a particular example of the geometry of the configuration under consideration: a y-invariant doubly layered insulator-metal structure. An insulator (e.g., vacuum) with refractive index $n^{(u)} = 1$ occupies the domain above the graph $z = g(x)$,

$$S^{(u)} := \{z > g(x)\},$$

and a second material (e.g., a metal) with index of refraction $n^{(w)}$ fills

$$S^{(w)} := \{z < g(x)\}.$$

The grating is d-periodic so that $g(x + d) = g(x)$. The structure is illuminated from above by monochromatic plane-wave incident radiation of angular frequency ω, aligned with the grooves

$$\begin{pmatrix} \underline{\mathbf{E}}^i(x,z,t) \\ \underline{\mathbf{H}}^i(x,z,t) \end{pmatrix} = \begin{pmatrix} \mathbf{A} \\ \mathbf{B} \end{pmatrix} e^{i\alpha x - i\gamma z - i\omega t}.$$

We consider the reduced total electric and magnetic fields

$$\begin{pmatrix} \mathbf{E}(\mathbf{x},\mathbf{z}) \\ \mathbf{H}(\mathbf{x},\mathbf{z}) \end{pmatrix} = \begin{pmatrix} \underline{\mathbf{E}}(x,z,t) \\ \underline{\mathbf{H}}(x,z,t) \end{pmatrix} e^{i\omega t},$$

which, like the reduced scattered fields, are α - quasiperiodic due to the incident radiation. Finally, the scattered radiation must be "outgoing" (upward propagating in $S^{(u)}$ and downward propagating in $S^{(w)}$).

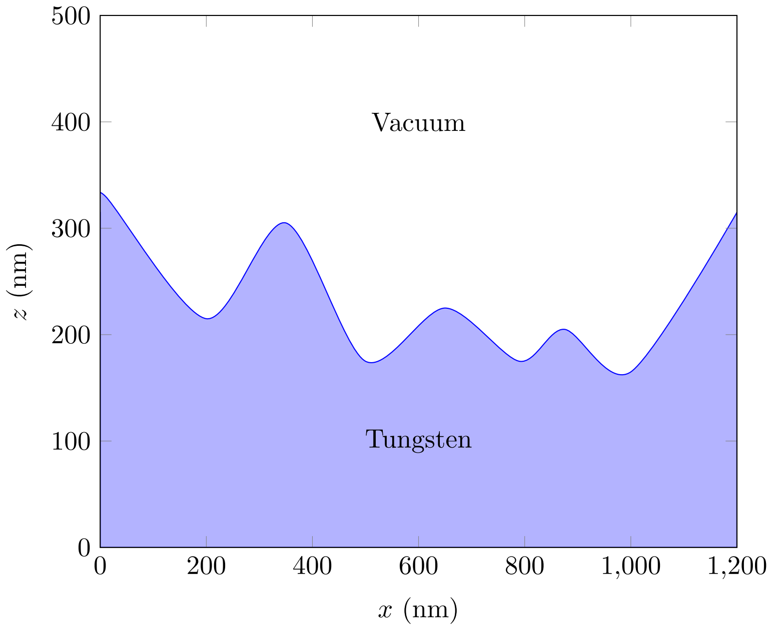

FIGURE 1. A vacuum-tungsten structure with d-periodic interface.

As shown in [**92**], and discussed in the preceding chapter, in this two-dimensional setting the time-harmonic Maxwell equations decouple into two scalar Helmholtz problems which govern the transverse electric (TE) and transverse magnetic (TM) polarizations. We denote the invariant (y) directions of the scattered (electric or magnetic) fields by

$$u = u(x,z), \quad w = w(x,z),$$

in $S^{(u)}$ and $S^{(w)}$, respectively, and the incident radiation in the upper layer specified by u^i. We are led to seek outgoing, α-quasiperiodic solutions of

$$\Delta u + \left(k^{(u)}\right)^2 = 0, \qquad z > g(x), \tag{102a}$$

$$\Delta w + \left(k^{(w)}\right)^2 = 0, \qquad z < g(x), \tag{102b}$$

$$u - w = \zeta, \qquad z = g(x), \tag{102c}$$

$$\partial_{\mathbf{n}} u - \tau^2 \partial_{\mathbf{n}} w = \psi, \qquad z = g(x), \tag{102d}$$

where $k^{(m)} = n^{(m)}\omega/c, (m \in \{u, w\}), \mathbf{n} = (-\partial_x g, 1)^T$, the Dirichlet and Neumann data are

$$\begin{aligned} \zeta(x) &:= -u^i(x, g(x)) = -e^{i\alpha x - i\gamma^{(u)} g(x)}, \\ \psi(x) &:= -(\partial_{\mathbf{n}} u^i)(x, g(x)) \\ &= (i\gamma^{(u)} + i\alpha(\partial_x g))e^{i\alpha x - i\gamma^{(u)} g(x)}, \end{aligned}$$

and we have the following for TE and TM cases:

$$\tau^2 = \begin{cases} 1 & \text{TE,} \\ (k^{(u)}/k^{(u)})^2 = (n^{(u)}/n^{(w)})^2 & \text{TM.} \end{cases}$$

1.1. Transparent Boundary Conditions. We recall [**92**] that for $z > \|g\|_\infty$, outgoing solutions in $S^{(u)}$ can be expressed as

$$u(x, z) = \sum_{p \in \mathbb{Z}} \hat{u}_p e^{i\alpha_p x + i\gamma_p^{(u)} z}, \tag{103}$$

for appropriately "propagating modes." Establishing an "artificial boundary" at $z = a > \|g\|_\infty$ with corresponding Dirichlet data $u_a := u(x, a)$, then it is clear that

$$u(x, z) = \sum_{p \in \mathbb{Z}} \hat{u}_{a,p} e^{i\alpha_p x + i\gamma_p^{(u)} (z-a)}. \tag{104}$$

Using this we compute the Neumann data, $\widetilde{u}_a(x) := -(\partial_z u)(x, a)$,

$$\widetilde{u}_a(x) = \sum_{p \in \mathbb{Z}} (-i\gamma_p^{(u)}) \hat{u}_{a,p} e^{i\alpha_p x}, \tag{105}$$

and define the DNO

$$T^{(u)}[u_a(x)] = \sum_{p \in \mathbb{Z}} (-i\gamma_p^{(u)}) \hat{u}_{a,p} e^{i\alpha_p x}. \tag{106}$$

Using this we may enforce the OWC at the artificial boundary using

$$\partial_z u + T^{(u)} u = 0, \;\; z = a. \tag{107}$$

A similar method using an artificial boundary $z = -b < \|g\|_\infty$ enables us to satisfy an OWC for downward propagation

$$\partial_z u + T^{(w)} u = 0, \ z = -b. \tag{108}$$

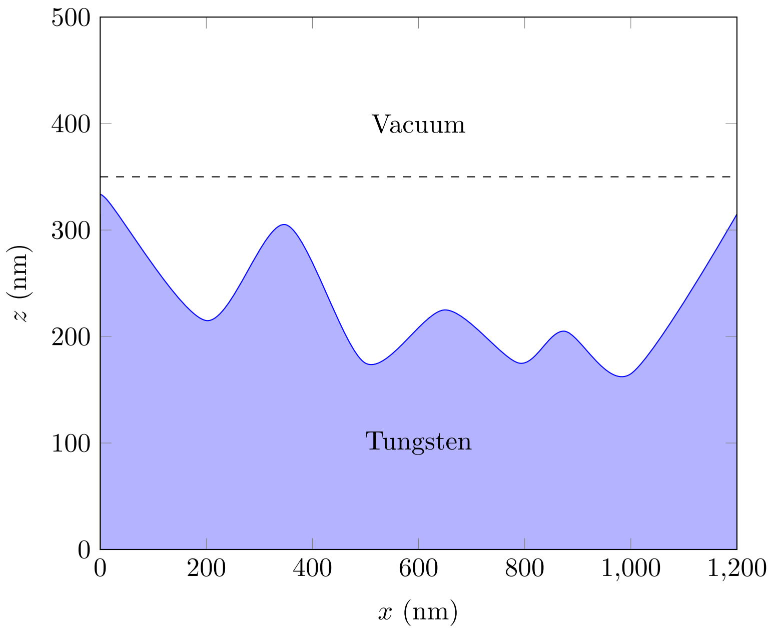

FIGURE 2. A vacuum-tungsten structure with d-periodic interface and artificial boundary layer at $z = a = 350$ nm.

1.2. Far-Field Observation. While we advocate an inversion strategy based upon "far field" data measured quite near the unknown grating interface (giving rise to "near field measurement") it is unreasonable to expect on-surface measurements. To specify the data which we deem relevant we again consider the artificial boundary $z = a$ and the far field pattern, $u_a(x)$. There is a well-defined map

$$L : U \to u_a,$$

where $U = u(x, g(x))$, which has a severely ill-conditioned inverse reflecting the fundamental ill-posedness of this inverse problem.

2. Boundary Formulation

We now specify a non-overlapping Domain Decomposition Method (DDM) reformulation of our problem in terms of the (upper and lower) Dirichlet traces

$$U(x) := [u]_{z=g}, \quad W(x) := [w]_{z=g},$$

and their (exterior pointing, upper and lower) Neumann analogues

$$\widetilde{U}(x) := [-\partial_{\mathbf{n}} u]_{z=g} = [-\partial_z u + (\partial_x g)\partial_x u]_{z=g},$$

$$\widetilde{W}(x) := [\partial_{\mathbf{n}} w]_{z=g} = [\partial_z w - (\partial_x g)\partial_x w]_{z=g},$$

The governing equations, (50), are equivalent to

$$U - W = \zeta, \ -\widetilde{U} - \tau^2 \widetilde{W} = \psi. \tag{109}$$

These two equations for four unknowns can be re-expressed in terms of two unknowns by using Dirichlet-Neumann Operators.

DEFINITION 2.1. *Given a sufficiently smooth deformation $g(x)$, the unique quasiperiodic solution of*

$$\Delta u + \left(k^{(u)}\right)^2 = 0, \qquad z > g(x), \tag{110a}$$

$$u = U, \qquad z = g(x), \tag{110b}$$

$$\partial_z u + T^{(u)} = 0, \qquad z = a, \tag{110c}$$

defines the Dirichlet-Neumann Operator

$$G[U] = G(g)[U] := \widetilde{U}. \tag{111}$$

In a similar fashion we have:

DEFINITION 2.2. *Given a sufficiently smooth deformation $g(x)$, the unique quasiperiodic solution of*

$$\Delta w + \left(k^{(w)}\right)^2 = 0, \qquad -b < z < g(x), \tag{112a}$$

$$w = W, \qquad z = g(x), \tag{112b}$$

$$\partial_z w - T^{(w)} = 0, \qquad z = -b, \tag{112c}$$

defines the Dirichlet-Neumann Operator

$$J[W] = J(g)[W] := \widetilde{W}. \tag{113}$$

In terms of these (109) becomes

$$U - W = \zeta, \quad -G[U] - \tau^2 J[W] = \psi,$$

and using the first equation to eliminate $W = U - \zeta$, we find

$$(G + \tau^2 J)[U] = -\psi + \tau^2 J[\zeta]. \tag{114}$$

3. The Forward Problem

We now pause to carefully define our "forward problem" so that our inversion strategy can be clearly stated. To begin, as we noted in the Introduction, the nature of the problem which we seek to simulate gives us a wealth of information. More specifically we know:

1. The structure is doubly layered so we need to identify only the single interface $z = g(x)$.

2. The composition of the two layers are known: Vacuum above a known material (a dielectric, or a metal such as silver or gold). So, we can consider $n^{(u)}$ and $n^{(w)}$ as knowns.

3. The period of the interface, d, and the mean observation distance, a, are known. This is not strictly true, but we assume that the error in these measurements is much less than that of other mistakes we make.

In any experiment we can vary the angle, θ, and wavelength, λ, of the incident radiation, $u^i(x, z)$. From this we define the wavenumbers

$$k_0 = 2\pi/\lambda, \quad k^{(u)} = n^{(u)} k_0, \quad k^{(w)} = n^{(w)} k_0,$$

which give

$$\alpha = k^{(u)} \sin(\theta), \quad \gamma^{(u)} = k^{(u)} \cos(\theta), \quad \gamma^{(w)} = k^{(w)} \cos(\theta).$$

For the forward problem we consider the interface $g(x)$ as input, and view the far-field pattern, $u_a(x)$, as the output, and denote F the forward map

$$F : g \to u_a(x),$$

An evaluation of this function amounts to solving the two equations

$$(G+\tau^2 J)U = -\psi + \tau^2 J[\zeta], \tag{115a}$$

$$u_a = L[U], \tag{115b}$$

or

$$u_a = L\left[(G+\tau^2 J)^{-1}\left[-\psi + \tau^2 J[\zeta]\right]\right]. \tag{116}$$

We recall that there are a wide array of numerical methods for evaluating this map including volumetric schemes such as Finite Difference [**63**], Finite Element [**58**], Spectral Element [**34**], and Spectral Methods [**42**], [**97**], to surface methods like Boundary Integral Methods [**31**], [**96**]; however we select the Method of Field Expansions (FE).

3.1. The Method of Field Expansions. We now specify the FE recursions to simulate solutions of (110) and (112), and compute the DNOs (111) and (113). We recall that the approach begins with the assumption that the shape of the interface deformation $g(x)$ satisfies

$$g(x) = \varepsilon f(x),\ \varepsilon \ll 1,$$

with f sufficiently smooth. With this assumption the fields and DNOs can be shown to depend analytically upon the deformation size ε so that

$$u(x,z,\varepsilon) = \sum_{n=0}^{\infty} u_n(x,z)\varepsilon^n,\ w(x,z,\varepsilon) = \sum_{n=0}^{\infty} w_n(x,z)\varepsilon^n, \tag{117}$$

and

$$G(\varepsilon) = \sum_{n=0}^{\infty} G_n\varepsilon^n,\ J(\varepsilon) = \sum_{n=0}^{\infty} J_n\varepsilon^n. \tag{118}$$

As we have seen, to derive useful forms for the coefficients $\{u_n, w_n, G_n, J_n\}$, we substitute the previous expansions from the first chapter into (117) and (118) which yields a corresponding boundary value problem for each n providing a method to recursively determine each of the $\{\hat{u}_{n,p}, \hat{w}_{n,p}, \hat{G}_{n,p}, \hat{J}_{n,p}\}$ with the respective order zero coefficients given by

$$\hat{U}_p, \hat{W}_p, \hat{G}_p,\ \text{and}\ \hat{J}_p.$$

4. The Inverse Problem

We are now in a position to specify our inversion strategy. As we noted above, we are safe in assuming that much is already known: A doubly layered structure separated by an unknown interface, $z = g(x)$, with known refractive indices, $\{n^{(u)}, n^{(w)}\}$, period, d, and mean observation distance, a. Thus, we set ourselves the problem of finding $g(x)$ given a collection of observation triples

$$\{\theta^j, \lambda^j, u_a^j(x)\}, \quad j = 1, ..., J.$$

We adopt a nonlinear least squares philosophy [**59**], [**91**] and seek to minimize the residual

$$R(g) := \begin{pmatrix} (G + \tau^2 J)U + \psi - \tau^2 J[\zeta] \\ u_a - L[U] \end{pmatrix}. \tag{119}$$

Among several strategies we considered for this task, the most rewarding were the Gauss-Newton (GN) approach, and the Levenberg-Marquardt (LM) algorithm. Each of these is an iterative strategy which, given an initial guess, x_0, updates the current iterate, x_k, by adding a correction, v_k, to give a better approximation

$$x_{k+1} = x_k + v_k.$$

In the case of GN, the correction solves the least-squares system

$$J^T J v_k = -JR(x_k), \quad J = R'(x_k).$$

By constrast, LM considers a "regularized" system

$$Bv_k = -JR(x_k), \quad B = J^T J + \lambda_k \text{diag}[J^T J], \quad J = R'(x_k),$$

and $\lambda_k \geq 0$ is chosen adaptively based upon the ratio of actual to predicted reduction in the objective function $R^T R$ [**59**], [**91**].

5. Numerical Results

We now demonstrate the efficiency of our algorithm by comparing our results for both the GN and LM methods to those reported in [**68**] by matching the chosen profiles and parameters when appropriate. We begin with the two-dimensional GN method.

5.1. Results with Gauss-Newton Method. For the first experiment employing the GN method, we considered the profile given by

$$g(x) = \varepsilon e^{\cos(2x)}, \tag{120}$$

which is a 2π-periodic analytic function separating a dielectric material with $k^{(u)} = 1.1$ and a perfectly electric conductor. After implementing our forward solver to generate an approximate solution u_a at the transparent boundary $z = a = 1$ with $N_x = 32$ grid points and a Taylor Expansion of order $N = 10$, we used the GN method to simulate the data at the interface. Emulating the tables given in [**68**] we report our results in table 1 which shows that the rate of convergence is superior to the rate reported by [**68**] at the cost of a digit of accuracy. The results reported in table 2 provide results with higher perturbation sizes which were beyond the capability of the method in [**68**].

ε	Iterations	Absolute L^∞ Error	Relative L^∞ Error
0.001	2	5.12385×10^{-9}	1.88496×10^{-6}
0.002	2	1.70321×10^{-8}	3.13287×10^{-6}
0.003	2	2.29475×10^{-8}	2.81398×10^{-6}
0.004	2	1.82473×10^{-8}	1.6782×10^{-6}
0.005	2	1.48634×10^{-8}	1.09359×10^{-6}
0.006	2	6.86197×10^{-8}	4.2073×10^{-6}
0.007	2	4.92943×10^{-8}	2.59062×10^{-6}
0.008	2	8.3038×10^{-8}	3.81849×10^{-6}
0.009	2	5.53309×10^{-8}	2.26168×10^{-6}
0.010	2	4.17534×10^{-8}	1.53602×10^{-6}

TABLE 1. Comparison of absolute and relative L^∞ errors of Gauss-Newton method for $f(x) = \varepsilon e^{\cos(2x)}$ with physical parameters $\alpha = 0$, $\gamma = 1.1$, $d = 2\pi$, $a = 1$, and absolute error tolerance $\tau = 10^{-7}$.

ε	Iterations	Absolute L^∞ Error	Relative L^∞ Error
0.01	2	4.17534×10^{-8}	1.53602×10^{-6}
0.02	3	1.33778×10^{-8}	2.4607×10^{-7}
0.03	3	8.09949×10^{-9}	9.93212×10^{-8}
0.04	3	1.41296×10^{-8}	1.2995×10^{-7}
0.05	3	1.69508×10^{-8}	1.24717×10^{-7}
0.06	3	4.84962×10^{-9}	2.97346×10^{-8}
0.07	3	7.78258×10^{-9}	4.09007×10^{-8}
0.08	3	1.48791×10^{-8}	6.84214×10^{-8}
0.09	3	6.35049×10^{-9}	2.59579×10^{-8}
0.10	3	9.92956×10^{-9}	3.65288×10^{-8}

TABLE 2. Absolute and relative L^∞ errors of Gauss-Newton method for $f(x) = \varepsilon e^{\cos(2x)}$ with physical parameters $\alpha = 0$, $\gamma = 1.1$, $d = 2\pi$, $a = 1$, and absolute error tolerance $\tau = 10^{-7}$.

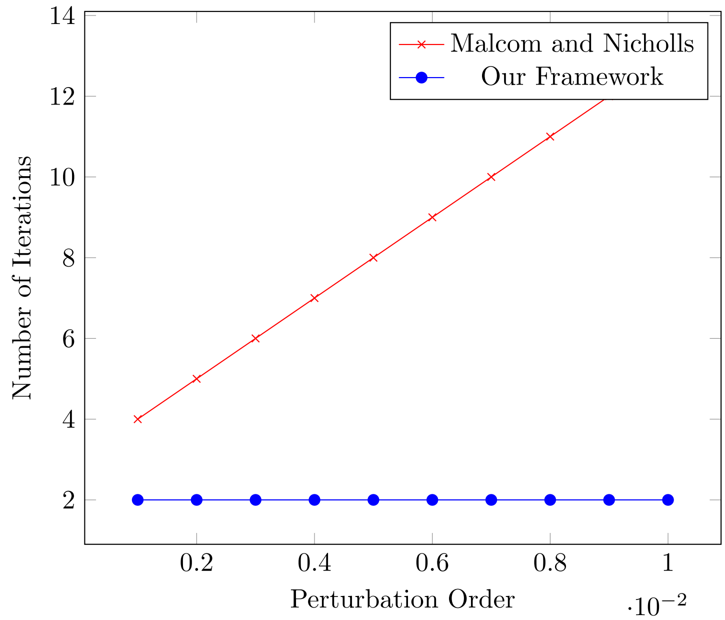

FIGURE 3. Comparison of number of iterations as a function of perturbation order of 2d Gauss-Newton method for $f(x) = \varepsilon e^{\cos(2x)}$.

The next two profiles under consideration were chose based upon their utility in modeling underwater features [**89**] which were also tested in [**68**]. The function

$$g(x) = \varepsilon \operatorname{sech}(2x), \tag{121}$$

was chosen to model a Gaussian pulse (see Figure 4), and

$$g(x) = \varepsilon(\tanh(2(x + 3\pi/5)) - \tanh(2(x - 3\pi/5))), \tag{122}$$

was chosen to model a sandbar (see Figure 5).

For each of these profiles we let $\alpha = 0.02$ and $\gamma = 1.3$, and again took $N_x = 32$ equally-spaced grid points with a Taylor expansion of order $N = 10$. As before, we implement GN to simulate the interface data and report our results in tables 3, 4, 5, and 6. As with our preceding analytic and periodic interface, we observe a rapid convergence rate far superior to the rate reported in [**68**] at the cost of a digit of accuracy (see Figures 6 and 7).

5.2. Results with Levenberg-Marquardt Method. For our LM experiments, we employed the same profiles and physical parameters for our experiments involving the GN method. The results reported for each of the chosen interfaces in tables 7, 8, 9,10,11, and 12 show that while the rate of

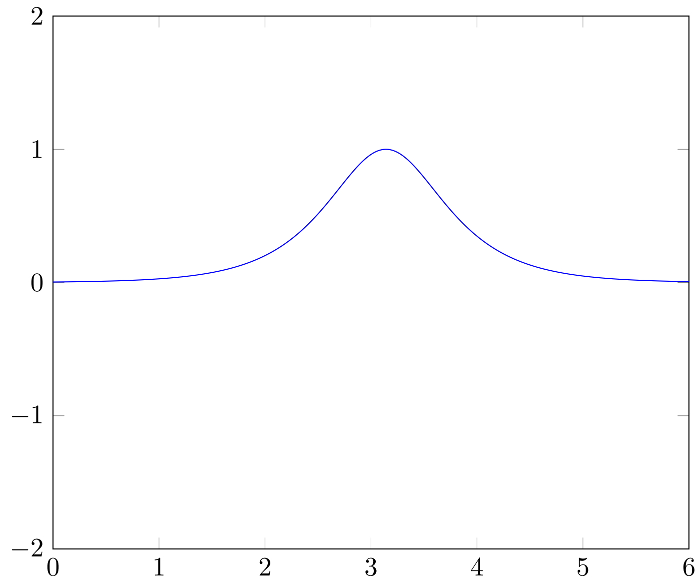

FIGURE 4. Problem configuration with interface $g(x) = \mathrm{sech}(2(x - \pi))$.

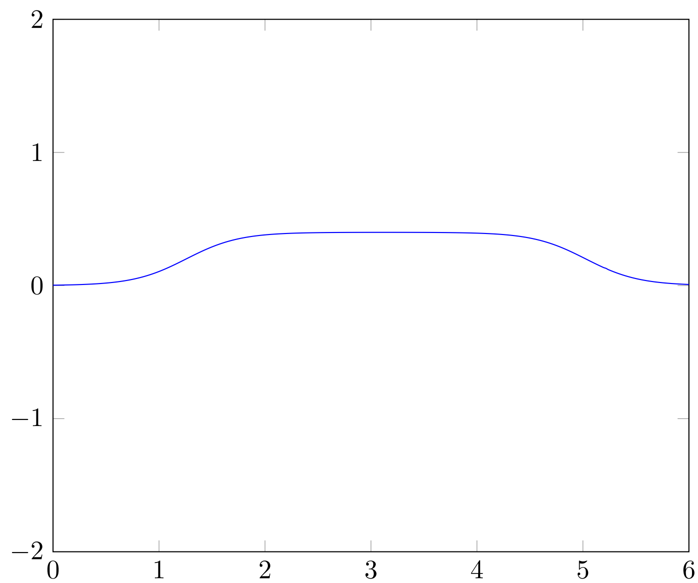

FIGURE 5. Problem configuration with interface $g(x) = 0.2(\tanh(2(x + 3\pi/5)) - \tanh(2(x - 3\pi/5)))$.

convergence is slightly slower than those resulting from the GN method they are still vastly superior to those reported in [**68**] (see Figures 8 - 10).

Given the strength of these initial experiments, we decided to investigate the convergence rate of our NLS-based methodology in the case of a crossed, biperiodic surface.

ε	Iterations	Absolute L^∞ Error	Relative L^∞ Error
0.001	2	6.53059×10^{-9}	6.53059×10^{-6}
0.002	2	1.44806×10^{-8}	7.24031×10^{-6}
0.003	2	1.80531×10^{-8}	6.01771×10^{-6}
0.004	2	2.54028×10^{-8}	6.3507×10^{-6}
0.005	2	5.6527×10^{-9}	1.13054×10^{-6}
0.006	2	1.37405×10^{-8}	2.29009×10^{-6}
0.007	2	8.75834×10^{-9}	1.25119×10^{-6}
0.008	2	7.07984×10^{-9}	8.8498×10^{-7}
0.009	2	2.23095×10^{-8}	2.47883×10^{-6}
0.010	2	3.29825×10^{-8}	3.29825×10^{-6}

TABLE 3. Comparison of absolute and relative L^∞ errors of Gauss-Newton method for $f(x) = \varepsilon \text{sech}(2x)$ with physical parameters $\alpha = 0.2$, $\gamma = 1.3$, $d = 2\pi$, $a = 1$, and absolute error tolerance $\tau = 10^{-7}$.

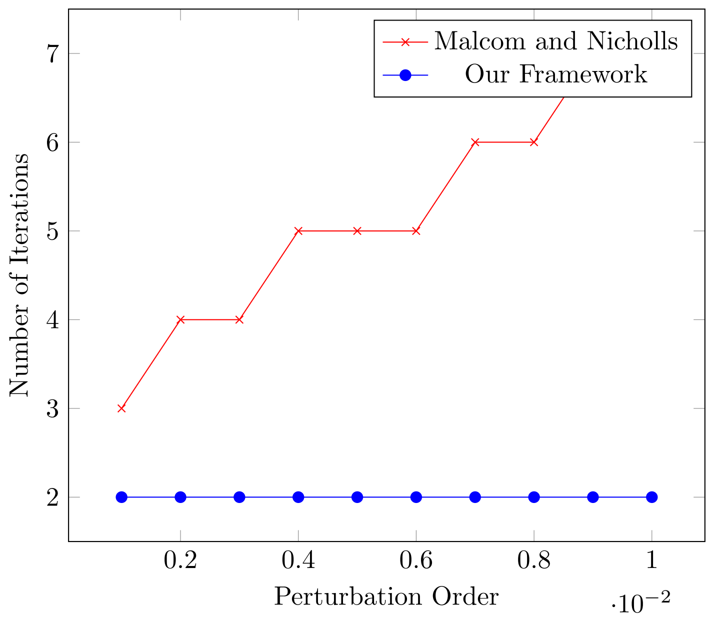

FIGURE 6. Comparison of number of iterations as a function of perturbation order of Gauss-Newton method for $f(x) = \varepsilon \text{sech}(2x)$.

5.3. Biperiodic Surfaces in Three-Dimensional Structures. Using the 2π-biperiodic surface

$$g(x) = \varepsilon e^{\cos(2x)+\cos(2y)}, \tag{123}$$

with physical parameters $\alpha = 0.1$, $\beta = 0.2$, and $\gamma^{(u)} = 1.21$ over $N_x = N_y = 24$ equally-spaced gridpoints and a Taylor expansion of order $N = 10$, we set an absolute error tolerance of $\tau = 10^{-6}$ and report our results with GN and LM. We see that our NLS methodologies retain a rapid rate of convergence despite a higher dimensional interface structure.

ε	Iterations	Absolute L^∞ Error	Relative L^∞ Error
0.01	2	3.29825×10^{-8}	3.29825×10^{-6}
0.02	2	3.10684×10^{-8}	1.55342×10^{-6}
0.03	2	5.45511×10^{-8}	1.81837×10^{-6}
0.04	2	5.40971×10^{-8}	1.35243×10^{-6}
0.05	3	1.45434×10^{-8}	2.90869×10^{-7}
0.06	3	1.0168×10^{-8}	1.69467×10^{-7}
0.07	3	9.11842×10^{-8}	1.30263×10^{-6}
0.08	3	1.01959×10^{-8}	1.27449×10^{-7}
0.09	3	1.01747×10^{-8}	1.13053×10^{-7}
0.10	3	3.38578×10^{-9}	3.38578×10^{-8}

TABLE 4. Absolute and relative L^∞ errors of Gauss-Newton method for $f(x) = \varepsilon \operatorname{sech}(2x)$ with physical parameters $\alpha = 0.2$, $\gamma = 1.3$, $d = 2\pi$, $a = 1$, and absolute error tolerance $\tau = 10^{-7}$.

ε	Iterations	Absolute L^∞ Error	Relative L^∞ Error
0.001	2	2.1134×10^{-8}	1.05783×10^{-5}
0.002	2	1.85757×10^{-8}	4.64886×10^{-6}
0.003	2	1.16117×10^{-8}	1.93734×10^{-6}
0.004	2	2.2996×10^{-8}	2.87755×10^{-6}
0.005	2	7.3449×10^{-8}	7.35271×10^{-6}
0.006	2	6.2667×10^{-8}	5.2278×10^{-6}
0.007	2	6.72537×10^{-8}	4.80894×10^{-6}
0.008	2	4.65598×10^{-8}	2.91309×10^{-6}
0.009	2	7.12626×10^{-8}	3.96324×10^{-6}
0.010	2	4.89571×10^{-8}	2.45046×10^{-6}

TABLE 5. Comparison of absolute and relative L^∞ errors of Gauss-Newton method for $f(x) = \varepsilon(\tanh(2(x + 3\pi/5)) - \tanh(2(x - 3\pi/5)))$ with physical parameters $\alpha = 0.2$, $\gamma = 1.3$, $d = 2\pi$, $a = 1$, and absolute error tolerance $\tau = 10^{-7}$.

ε	Iterations	Absolute L^∞ Error	Relative L^∞ Error
0.01	2	4.89571×10^{-8}	2.45046×10^{-6}
0.02	3	1.3441×10^{-8}	4.64886×10^{-6}
0.03	3	9.33326×10^{-9}	1.5572×10^{-7}
0.04	3	8.14999×10^{-9}	1.01983×10^{-7}
0.05	3	5.14035×10^{-9}	5.14582×10^{-8}
0.06	3	5.96408×10^{-9}	4.97535×10^{-8}
0.07	3	3.86656×10^{-9}	2.76477×10^{-8}
0.08	3	6.73874×10^{-9}	4.21619×10^{-8}
0.09	3	4.2248×10^{-9}	2.34961×10^{-8}
0.10	3	7.67753×10^{-9}	3.84285×10^{-8}

TABLE 6. Absolute and relative L^∞ errors of Gauss-Newton method for $f(x) = \varepsilon(\tanh(2(x+3\pi/5)) - \tanh(2(x-3\pi/5)))$ with physical parameters $\alpha = 0.2$, $\gamma = 1.3$, $d = 2\pi$, $a = 1$, and absolute error tolerance $\tau = 10^{-7}$.

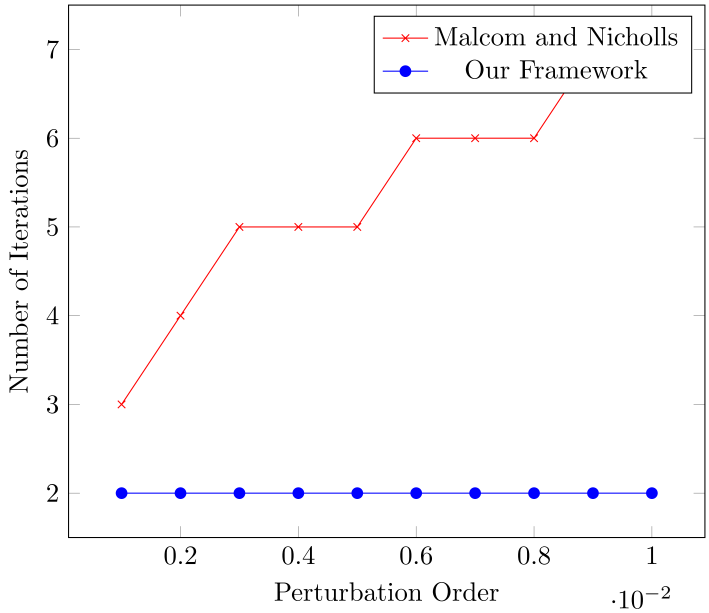

FIGURE 7. Comparison of number of iterations as a function of perturbation order of Gauss-Newton method for $f(x) = \varepsilon(\tanh(2(x + 3\pi/5)) - \tanh(2(x - 3\pi/5)))$.

ε	Iterations	Absolute L^∞ Error	Relative L^∞ Error
0.001	2	7.04262×10^{-9}	2.59084×10^{-6}
0.002	2	1.2649×10^{-8}	2.32666×10^{-6}
0.003	2	4.30004×10^{-8}	5.27299×10^{-6}
0.004	3	5.56464×10^{-9}	5.11779×10^{-7}
0.005	3	3.04016×10^{-9}	2.23683×10^{-7}
0.006	3	3.30447×10^{-9}	2.02608×10^{-7}
0.007	3	6.61107×10^{-9}	3.4744×10^{-7}
0.008	3	2.83708×10^{-9}	1.30463×10^{-7}
0.009	3	3.65685×10^{-9}	1.49475×10^{-7}
0.010	3	4.73347×10^{-9}	1.74134×10^{-7}

TABLE 7. Comparison of absolute and relative L^∞ errors of Levenberg-Marquardt method for $f(x) = \varepsilon e^{\cos(2x)}$ with physical parameters $\alpha = 0$, $\gamma = 1.1$, $d = 2\pi$, $a = 1$, and absolute error tolerance $\tau = 10^{-7}$.

ε	Iterations	Absolute L^∞ Error	Relative L^∞ Error
0.01	2	8.59926×10^{-8}	3.16349×10^{-6}
0.02	3	2.03003×10^{-9}	3.73404×10^{-8}
0.03	3	5.92628×10^{-9}	7.26719×10^{-8}
0.04	3	1.80464×10^{-8}	1.65973×10^{-7}
0.05	3	5.78422×10^{-8}	4.25579×10^{-7}
0.06	4	1.37597×10^{-8}	8.43649×10^{-8}
0.07	4	1.10804×10^{-8}	5.82324×10^{-8}
0.08	4	1.10195×10^{-8}	5.06729×10^{-8}
0.09	4	8.06238×10^{-9}	3.29554×10^{-8}
0.10	4	1.38966×10^{-8}	5.11227×10^{-8}

TABLE 8. Absolute and relative L^∞ errors of Levenberg-Marquardt method for $f(x) = \varepsilon e^{\cos(2x)}$ with physical parameters $\alpha = 0$, $\gamma = 1.1$, $d = 2\pi$, $a = 1$, and absolute error tolerance $\tau = 10^{-7}$.

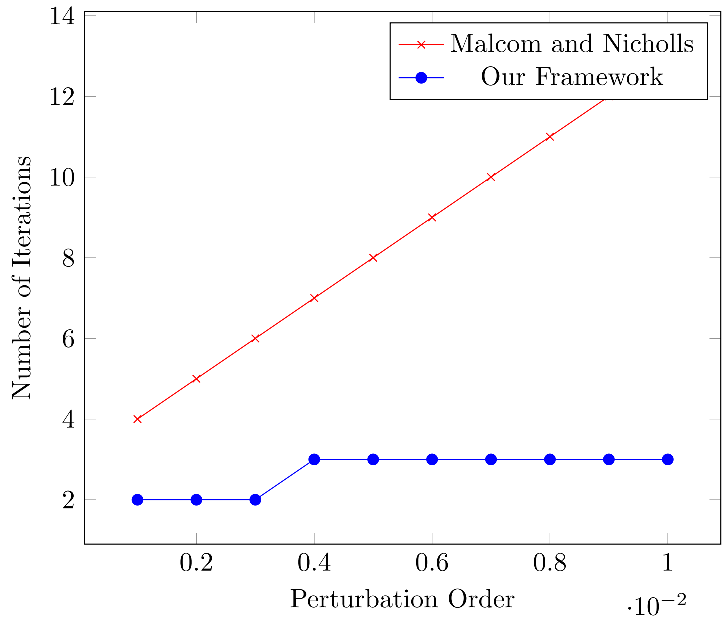

FIGURE 8. Comparison of number of iterations as a function of perturbation order of Levenberg-Marquardt method for $f(x) = \varepsilon e^{\cos(2x)}$.

ε	Iterations	Absolute L^∞ Error	Relative L^∞ Error
0.001	2	5.04942×10^{-9}	5.04942×10^{-6}
0.002	2	2.51027×10^{-8}	1.25513×10^{-5}
0.003	2	6.59102×10^{-8}	2.19701×10^{-5}
0.004	3	8.78783×10^{-9}	2.19696×10^{-6}
0.005	3	4.31915×10^{-9}	8.63831×10^{-7}
0.006	4	1.02421×10^{-8}	1.70702×10^{-6}
0.007	4	1.07042×10^{-8}	1.52916×10^{-6}
0.008	4	6.46297×10^{-9}	8.07871×10^{-7}
0.009	4	5.24258×10^{-9}	5.82509×10^{-7}
0.010	4	1.20323×10^{-8}	1.20323×10^{-6}

TABLE 9. Comparison of absolute and relative L^∞ errors of Levenberg-Marquardt method for $f(x) = \varepsilon \mathrm{sech}(2x)$ with physical parameters $\alpha = 0.2$, $\gamma = 1.3$, $d = 2\pi$, $a = 1$, and absolute error tolerance $\tau = 10^{-7}$.

ε	Iterations	Absolute L^∞ Error	Relative L^∞ Error
0.01	3	1.53242×10^{-8}	1.53242×10^{-6}
0.02	3	5.3662×10^{-9}	2.6831×10^{-7}
0.03	3	1.11801×10^{-8}	3.72669×10^{-7}
0.04	3	1.94143×10^{-8}	4.85359×10^{-7}
0.05	3	7.25992×10^{-8}	1.45198×10^{-6}
0.06	4	4.12845×10^{-9}	6.88075×10^{-8}
0.07	4	8.09638×10^{-9}	1.15663×10^{-7}
0.08	4	1.0433×10^{-8}	1.30413×10^{-7}
0.09	4	5.22884×10^{-9}	5.80982×10^{-8}
0.10	4	5.828×10^{-9}	5.828×10^{-8}

TABLE 10. Absolute and relative L^∞ errors of Levenberg-Marquardt method for $f(x) = \varepsilon \mathrm{sech}(2x)$ with physical parameters $\alpha = 0.2$, $\gamma = 1.3$, $d = 2\pi$, $a = 1$, and absolute error tolerance $\tau = 10^{-7}$.

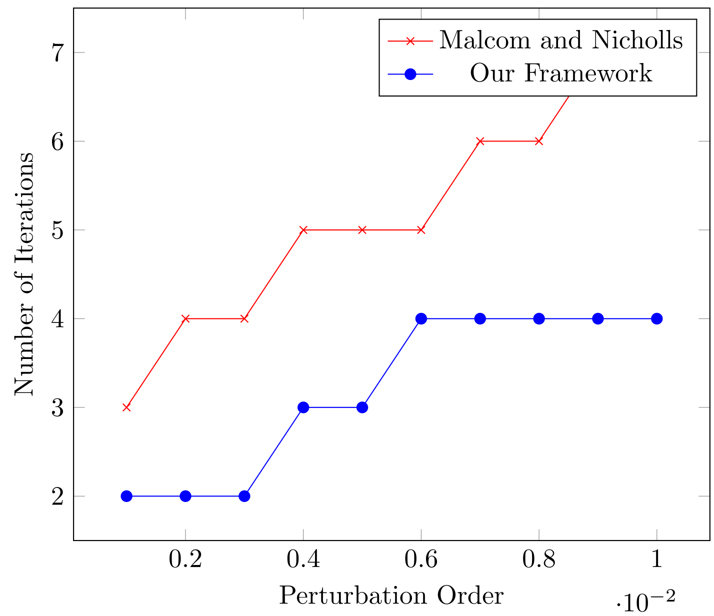

FIGURE 9. Comparison of number of iterations as a function of perturbation order of Levenberg-Marquardt method for $f(x) = \varepsilon \text{sech}(2x)$.

ε	Iterations	Absolute L^∞ Error	Relative L^∞ Error
0.001	3	6.55021×10^{-9}	3.27859×10^{-6}
0.002	3	1.35846×10^{-8}	3.39976×10^{-6}
0.003	3	4.75449×10^{-9}	7.93258×10^{-7}
0.004	3	1.10139×10^{-8}	1.3782×10^{-6}
0.005	3	2.93964×10^{-9}	2.94276×10^{-7}
0.006	3	1.1869×10^{-8}	9.90133×10^{-7}
0.007	3	7.57871×10^{-9}	5.41912×10^{-7}
0.008	3	9.76948×10^{-9}	6.11242×10^{-7}
0.009	3	2.21945×10^{-8}	1.23434×10^{-6}
0.010	3	1.82724×10^{-8}	9.14593×10^{-7}

TABLE 11. Comparison of absolute and relative L^∞ errors of Levenberg-Marquardt method for $f(x) = \varepsilon(\tanh(2(x + 3\pi/5)) - \tanh(2(x - 3\pi/5)))$ with physical parameters $\alpha = 0.2$, $\gamma = 1.3$, $d = 2\pi$, $a = 1$, and absolute error tolerance $\tau = 10^{-7}$.

ε	Iterations	Absolute L^∞ Error	Relative L^∞ Error
0.01	3	1.52832×10^{-8}	7.64973×10^{-7}
0.02	3	5.46978×10^{-9}	1.3689×10^{-7}
0.03	4	1.14338×10^{-8}	1.90766×10^{-7}
0.04	4	8.37588×10^{-9}	1.0481×10^{-7}
0.05	4	6.98388×10^{-9}	6.99131×10^{-8}
0.06	4	2.44196×10^{-8}	2.03713×10^{-7}
0.07	4	2.31178×10^{-8}	1.65303×10^{-7}
0.08	4	5.56971×10^{-8}	3.48477×10^{-7}
0.09	4	3.64979×10^{-8}	2.02982×10^{-7}
0.10	4	9.66565×10^{-8}	4.83797×10^{-7}

TABLE 12. Absolute and relative L^∞ errors of Levenberg-Marquardt method for $f(x) = \varepsilon(\tanh(2(x + 3\pi/5)) - \tanh(2(x - 3\pi/5)))$ with physical parameters $\alpha = 0.2$, $\gamma = 1.3$, $d = 2\pi$, $a = 1$, and absolute error tolerance $\tau = 10^{-7}$.

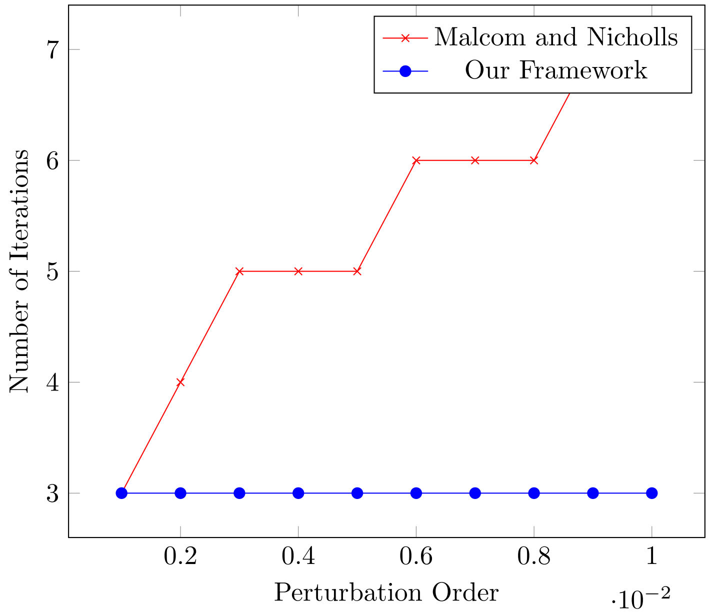

FIGURE 10. Comparison of number of iterations as a function of perturbation order of Levenberg-Marquardt method for $f(x) = \varepsilon(\tanh(2(x + 3\pi/5)) - \tanh(2(x - 3\pi/5)))$.

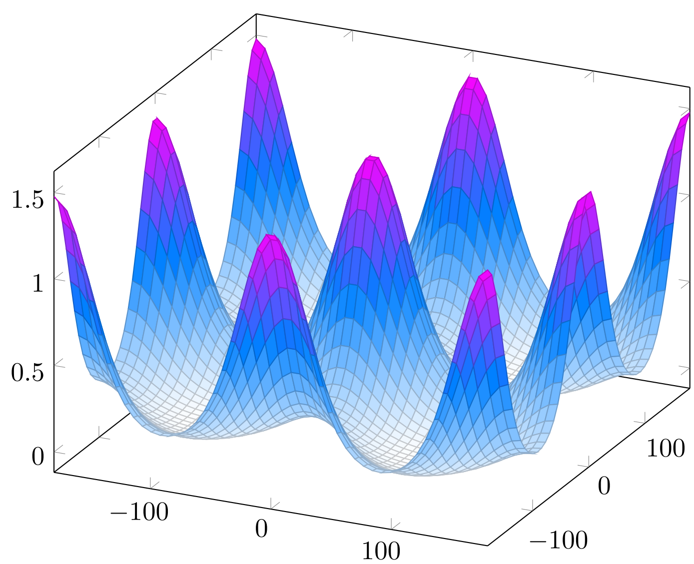

FIGURE 11. Problem configuration with interface $g(x) = 0.2e^{\cos(2x)+\cos(2y)}$.

ε	Iterations	Absolute L^∞ Error	Relative L^∞ Error
0.001	2	6.84782×10^{-8}	9.26752×10^{-6}
0.002	2	1.34678×10^{-7}	9.11337×10^{-6}
0.003	2	2.02256×10^{-7}	9.12415×10^{-6}
0.004	2	2.63101×10^{-7}	8.90171×10^{-6}
0.005	2	3.29993×10^{-7}	8.93193×10^{-6}
0.006	2	4.09238×10^{-7}	9.23072×10^{-6}
0.007	2	4.98737×10^{-7}	9.6424×10^{-6}
0.008	2	5.80323×10^{-7}	9.81727×10^{-6}
0.009	2	6.9363×10^{-7}	1.04303×10^{-5}
0.010	2	7.90182×10^{-7}	1.06939×10^{-5}

TABLE 13. Absolute and relative L^∞ errors of Gauss-Newton method for $f(x) = \varepsilon e^{\cos(2x)+\cos(2y)}$ with physical parameters $\alpha = 0$, $\gamma = 1.1$, $d = 2\pi$, $a = 1$, and absolute error tolerance $\tau = 10^{-6}$.

ε	Iterations	Absolute L^∞ Error	Relative L^∞ Error
0.001	3	5.44029×10^{-9}	7.36263×10^{-7}
0.002	3	5.60873×10^{-9}	3.7953×10^{-7}
0.003	3	2.7817×10^{-8}	1.25488×10^{-6}
0.004	3	1.1222×10^{-7}	3.79684×10^{-6}
0.005	3	3.88405×10^{-7}	1.0513×10^{-5}
0.006	4	4.58462×10^{-9}	1.0341×10^{-7}
0.007	4	5.20048×10^{-9}	1.00544×10^{-7}
0.008	4	4.91116×10^{-9}	8.30817×10^{-8}
0.009	4	1.033×10^{-8}	1.55335×10^{-7}
0.010	4	2.02177×10^{-8}	2.73617×10^{-7}

TABLE 14. Absolute and relative L^∞ errors of Levenberg-Marquardt method for $f(x) = \varepsilon e^{\cos(2x)+\cos(2y)}$ with physical parameters $\alpha = 0$, $\gamma = 1.1$, $d = 2\pi$, $a = 1$, and absolute error tolerance $\tau = 10^{-6}$.

CHAPTER 3

Conclusion

Through the implementation of a HOPS methodology we numerically simulated the solution to the Helmholtz equation, and used this solution within an NLS framework to solve the inverse problem of reconstruction of a periodic grating interface problem. Through comparison with results of [**68**], we have demonstrated that our numerical scheme coupling the FE method with both the GN and LM methods of solving nonlinear systems yields a simple, efficient, accurate, and superior method for reconstruction of a diffractive grating shape from far field measurements. Encouraged by our results, we extended our numerical methods to consider three-dimensional doubly-periodic grating surfaces which further suggests the robustness of our numerical methodology.

In consideration of future work inspired by the results presented here, we feel it is natural to consider extending our numerical philosophy from the two-dimensional scalar Helmholtz equation to the case of three-dimensional vector Maxwell Equations. We are confident that the flexibility of the HOPS methodology together with the simplicity of the NLS framework will again yield a simple, efficient, and accurate numerical scheme for solving the inverse diffraction grating problem.

Cited Literature

[1] Tilo Arens and Andreas Kirsch, *The factorization method in inverse scattering from periodic structures*, **Inverse Problems**, 19(5):1195–1211, 2003.

[2] Gang Bao, *A uniqueness theorem for an inverse problem in periodic diffractive optics*, **Inverse Problems**, 10(2):335–340, 1994.

[3] Gottfried Bruckner, Jin Cheng, and Masahiro Yamamoto, *An inverse problem in diffractive optics: conditional stability*, **Inverse Problems**, 18(2):415–433,2002.

[4] O. Bruno and B. Delourme, *Rapidly convergent two-dimensional quasi-periodic Green function throughout the spectrum including Wood anomalies*, **Journal of Computational Physics**, 262:262–290, 2014.

[5] Gottfried Bruckner and Johannes Elschner, *A two-step algorithm for the reconstruction of perfectly reflecting periodic profiles* **Inverse Problems**, 19(2):315–329, 2003.

[6] Jean-Pierre Bérenger, *A perfectly matched layer for the absorption of electromagnetic waves*, **J. Comput. Phys.**, 114(2):185–200, 1994.

[7] Jean-Pierre Bérenger, *Evanescent waves in PML's: origin of the numerical reflection in wave-structure interaction problems* **IEEE Trans. Antennas and Propagation**, 47(10):1497–1503, 1999.

[8] Gang Bao and Avner Friedman *Inverse problems for scattering by periodic structures*, **Arch. Rational Mech. Anal.**, 132(1):49–72, 1995.

[9] Oscar P. Bruno and Agustin G. Fernandez-Lado *Rapidly convergent quasiperiodic Green functions for scattering by arrays of cylinders including Wood anomalies*, **Proc. A.**, 473(2199):20160802, 23, 2017.

[10] A. Barnett and L. Greengard, *A new integral representation for quasi-periodic scattering problems in two dimensions*, **BIT Numerical Mathematics**, 51:67–90, 2011.

[11] George A. Baker, Jr. and Peter Graves-Morris, *Padé approximants*, **Cambridge University Press**, Cambridge, second edition, 1996.

[12] G. Bao, P. Li, and J. Lv, *Numerical solution of an inverse diffraction grating problem from phaseless data*, **J. Opt. Soc. Am. A**, 30:293–299, 2013.

[13] Oscar P. Bruno, Mark Lyon, Carlos Pérez-Arancibia, and Catalin Turc, *Windowed Green function method for layered-media scattering*, **SIAM J. Appl.Math.**, 76(5):1871–1898, 2016.

[14] G. Bao, P. Li, and H. Wu, *A computational inverse diffraction grating problem*, **J. Opt. Soc. Am. A**, 29:394–399, 2012.

[15] G. Bao, P. Li, and Y. Wang, *Near-field imaging with far-field data*, **Appl. Math. Lett.**, 60:36–42, 2016.

[16] *T. Binford, D. P. Nicholls, N. Nigam, and T. Warburton*, **Exact non reflecting boundary conditions on general domains and hp-finite elements**, Journal of Scientific Computing, 39(2):265–292, 2009.

[17] O. P. Bruno and C. Pérez-Arancibia, *Windowed Green function method for the Helmholtz equation in the presence of multiply layered media*, **Proc. A.**, 473(2202):20170161, 20, 2017.

[18] O. Bruno and F. Reitich, *Solution of a boundary value problem for the Helmholtz equation via variation of the boundary into the complex domain*, **Proc. Roy. Soc. Edinburgh Sect. A**, 122(3-4):317–340, 1992.

[19] O. Bruno and F. Reitich Numerical solution of diffraction problems: A method of variation of boundaries, **J. Opt. Soc. Am. A**, 10(6):1168–1175, 1993.

[20] O. Bruno and F. Reitich, *Numerical solution of diffraction problems: A method of variation of boundaries. II. Finitely conducting gratings, Padé approximants, and singularities*, **J. Opt. Soc. Am. A**, 10(11):2307–2316, 1993.

[21] O. Bruno and F. Reitich, *Numerical solution of diffraction problems: A method of variation of boundaries. III. Doubly periodic gratings*, **J. Opt. Soc. Am. A**,10(12):2551–2562, 1993.

[22] Oscar P. Bruno and Fernando Reitich, *Approximation of analytic functions: A method of enhanced convergence*, **Math. Comp.**, 63(207):195–213, 1994.

[23] Oscar P. Bruno and Fernando Reitich, *Calculation of electromagnetic scattering via boundary variations and analytic continuation*, **Appl. Comput. Electromagn. Soc. J.**, 11(1):17–31, 1996.

[24] Oscar P. Bruno and Fernando Reitich, *Boundary-variation solutions for bounded-obstacle scattering problems in three dimensions*, **J. Acoust. Soc. Am.**, 104(5):2579–2583, 1998.

[25] Oscar P. Bruno and Fernando Reitich, *High-order boundary perturbation methods*, **Mathematical Modeling in Optical Science**, volume 22, pages 71-109. SIAM, Philadelphia, PA, 2001. Frontiers in Applied Mathematics Series.

[26] Oscar P. Bruno, Stephen P. Shipman, Catalin Turc, and Stephanos Venakides, *Superalgebraically convergent smoothly windowed lattice sums for doubly periodic Green functions in three-dimensional space*, **Proc. A.**, 472(2191):20160255, 19, 2016.

[27] Min Hyun Cho and Alex Barnett, Robust fast direct integral equation solver for quasi-periodic scattering problems with a large number of layers, **Optics Express**, 23(2):1775–1799, 2015.

[28] Fioralba Cakoni and David Colton *A qualitative approach to inverse scattering theory*, **volume 188 of Applied Mathematical Sciences**, Springer, New York, 2014.

[29] Fioralba Cakoni, David Colton, and Houssem Haddar *Inverse scattering theory and transmission eigenvalues*, **volume 88 of CBMS-NSF Regional Conference Series in Applied Mathematics**, Society for Industrial and Applied Mathematics(SIAM), Philadelphia, PA, 2016.

[30] Fioralba Cakoni, David Colton, and Peter Monk, *The linear sampling method in inverse electromagnetic scattering*, **volume 80 of CBMS-NSF Regional Conference Series in Applied Mathematics**, Society for Industrial and Applied Mathematics(SIAM), Philadelphia, PA, 2011.

[31] D. Colton and R. Kress, *Inverse acoustic and electromagnetic scattering theory*, **Springer-Verlag**, Berlin, second edition, 1998.

[32] David Colton and Rainer Kress, *Inverse acoustic and electromagnetic scattering theory*, **volume 93 of Applied Mathematical Sciences**, Springer, New York, third edition, 2013.

[33] Ting Cheng, Peijun Li, and Yuliang Wang, *Near-field imaging of perfectly conducting grating surfaces*, **J. Opt. Soc. Am. A**, 30:2473–2481, 2013.

[34] M. O. Deville, P. F. Fischer, and E. H. Mund, *High-order methods for incompressible fluid flow*, **volume 9 of Cambridge Monographs on Applied and Computational Mathematics**. Cambridge University Press, Cambridge, 2002.

[35] S. Enoch and N. Bonod, *Plasmonics: From Basics to Advanced Topics*, **Springer Series in Optical Sciences**, Springer, New York, 2012.

[36] J. Elschner, G. C. Hsiao, and A. Rathsfeld, *Grating profile reconstruction based on finite elements and optimization techniques*, **SIAM J. Appl. Math.**, 64(2):525–545, 2003/04.

[37] T. W. Ebbesen, H. J. Lezec, H. F. Ghaemi, T. Thio, and P. A. Wolf, *Extraordinary optical transmission through sub-wavelength hole arrays*, **Nature**, 391(6668):667–669, 1998.

[38] J. Elschner and G. Schmidt, *Diffraction in periodic structures and optimal design of binary gratings. part i: Direct problems and gradient formulas*, **Math. Meth. Appl. Sci.**, 21:1297–1342, 1998.

[39] J. Elschner and G. Schmidt, *Numerical solution of optimal design problems for binary gratings*, **J. Comput. Phys.**, 146(2):603–626, 1998.

[40] Q. Fang, D. P. Nicholls, and J. Shen, *A stable, high-order method for three-dimensional bounded-obstacle scattering*, **J. Comput. Phys.**, 224(2):1145-1169,2007.

[41] D. Givoli, *Recent advances in the DtN FE method*, *Arch. Comput. Methods Engrg.*, 6(2):71-116, 1999.

[42] D. Gottlieb and S. A. Orszag, *Numerical analysis of spectral methods: theory and applications*, Society for Industrial and Applied Mathematics, Philadelphia, Pa., 1977. CBMS-NSF Regional Conference Series in Applied Mathematics, No.26.

[43] L. Greengard and V. Rokhlin, *A fast algorithm for particle simulations*, **J. Comput. Phys.**, 73(2):325–348, 1987.

[44] F. Hettlich, *Iterative regularization schemes in inverse scattering by periodic structures*, **Inverse Problems**, 18(3):701–714, 2002.

[45] F. Hettlich and A. Kirsch, *Schiffer's theorem in inverse scattering theory for periodic structures*, **Inverse Problems**, 13(2):351–361, 1997.

[46] B. Hu and D. P. Nicholls, *Analyticity of Dirichlet-Neumann operators on Hölder and Lipschitz domains*, **SIAM J. Math. Anal.**, 37(1):302–320, 2005.

[47] B. Hu and D. P. Nicholls, *The domain of analyticity of Dirichlet-Neumann operators*, **Proceedings of the Royal Society of Edinburgh A**, 140(2):367–389, 2010.

[48] Y. Hong and D. P. Nicholls, *A high-order perturbation of surfaces method for scattering of linear waves by periodic multiply layered gratings in two and three dimensions*, **Journal of Computational Physics**, 345:162–188, 2017.

[49] Y. Hong and D. P. Nicholls, *A stable high-order perturbation of surfaces method for numerical simulation of diffraction problems in triply layered media*, **Journal of Computational Physics**, 330:1043–1068, 2017.

[50] Y. Hong and D. P. Nicholls, *A high-order perturbation of surfaces method for vector electromagnetic scattering by doubly layered periodic crossed gratings.* **submitted**, 2018.

[51] J. Homola, *Surface plasmon resonance sensors for detection of chemical and biological species*, **Chemical Reviews**, 108(2):462–493, 2008.

[52] Hou De Han and Xiao Nan Wu, *Approximation of infinite boundary condition and its application to finite element methods*, **J. Comput. Math.**, 3(2):179–192, 1985.

[53] Jan S. Hesthaven and Tim Warburton, *Nodal discontinuous Galerkin methods*, **volume 54 of Texts in Applied Mathematics**, Springer, New York, 2008. Algorithms, analysis, and applications.

[54] H. Im, S. H. Lee, N. J. Wittenberg, T. W. Johnson, N. C. Lindquist, P. Nagpal, D. J. Norris, and S.-H. Oh, *Template-stripped smooth Ag nanohole arrays with silica shells for surface plasmon resonance biosensing*, **ACS Nano**, 5:6244–6253, 2011.

[55] J. Jose, L. R. Jordan, T. W. Johnson, S. H. Lee, N. J. Wittenberg, and S.-H. Oh, *Topographically at substrates with embedded nanoplasmonic devices for biosensing*, **Adv Funct Mater**, 23:2812–2820, 2013.

[56] X. Jiang and P. Li *Inverse electromagnetic diffraction by biperiodic dielectric gratings*, **Inverse Problems**, 33:085004, 2017.

[57] Claes Johnson and J.-Claude Nédélec, *On the coupling of boundary integral and finite element methods*, **Math. Comp.**, 35(152):1063–1079, 1980.

[58] Claes Johnson, *Numerical solution of partial differential equations by the finite element method*, **Cambridge University Press**, Cambridge, 1987.

[59] C. T. Kelley, *Iterative methods for optimization*, **volume 18 of Frontiers in Applied Mathematics**, Society for Industrial and Applied Mathematics (SIAM), Philadelphia, PA, 1999.

[60] Joseph B. Keller and Dan Givoli, *Exact nonreflecting boundary conditions*, **J. Comput. Phys.**, 82(1):172–192, 1989.

[61] Andreas Kirsch, *Uniqueness theorems in inverse scattering theory for periodic structures*, **Inverse Problems**, 10(1):145–152, 1994.

[62] Rainer Kress, *Linear integral equations*, **Springer-Verlag**, New York, third edition, 2014.

[63] Randall J. LeVeque, *Finite difference methods for ordinary and partial differential equations*, **Society for Industrial and Applied Mathematics (SIAM)**, Philadelphia, PA, 2007. Steady-state and time-dependent problems.

[64] N. C. Lindquist, T. W. Johnson, J. Jose, L. M. Otto, and S.-H. Oh, *Ultrasmooth metallic films with buried nanostructures for backside reflection-mode plasmonic biosensing*, **Annalen der Physik**, 524:687–696, 2012.

[65] S. A. Maier, *Plasmonics: Fundamentals and Applications*, **Springer**, New York, 2007.

[66] D. Michael Milder, *An improved formalism for rough-surface scattering of acoustic and electromagnetic waves*, **In Proceedings of SPIE - The International Society for Optical Engineering** (San Diego, 1991), volume 1558, pages 213– 221. Int. Soc. for Optical Engineering, Bellingham, WA, 1991.

[67] D. Michael Milder, *An improved formalism for wave scattering from rough surfaces*, **J. Acoust. Soc. Am.**, 89(2):529–541, 1991.

[68] A. Malcolm and D. P. Nicholls *A boundary perturbation method for recovering interface shapes in layered media*, **Inverse Problems**, 27(9):095009, 2011.

[69] A. Malcolm and D. P. Nicholls, *A field expansions method for scattering by periodic multilayered media*, **Journal of the Acoustical Society of America**, 129(4):1783–1793, 2011.

[70] A. Malcolm and D. P. Nicholls, *Operator expansions and constrained quadratic optimization for interface reconstruction: Impenetrable acoustic media*, **Wave Motion**, 51:23–40, 2014.

[71] M. Moskovits, *Surface-enhanced spectroscopy*, **Reviews of Modern Physics**, 57(3):783–826, 1985.

[72] D. Michael Milder and H. Thomas Sharp, *Efficient computation of rough surface scattering*, **In Mathematical and numerical aspects of wave propagation phenomena** (Strasbourg, 1991), pages 314–322. SIAM, Philadelphia, PA, 1991.

[73] D. Michael Milder and H. Thomas Sharp, *An improved formalism for rough surface scattering. ii: Numerical trials in three dimensions*, **J. Acoust. Soc. Am.**, 91(5):2620–2626, 1992.

[74] D. P. Nicholls, *A rapid boundary perturbation algorithm for scattering by families of rough surfaces* **Journal of Computational Physics**, 228(9):3405–3420, 2009.

[75] D. P. Nicholls *Three-dimensional acoustic scattering by layered media: A novel surface formulation with operator expansions implementation*, **Proceedings of the Royal Society of London**, A, 468:731–758, 2012.

[76] D. P. Nicholls, *A method of field expansions for vector electromagnetic scattering by layered periodic crossed gratings*, **Journal of the Optical Society of America, A**, 32(5):701–709, 2015.

[77] D. P. Nicholls *Numerical solution of diffraction problems: A high-order perturbation of surfaces/asymptotic waveform evaluation method* **SIAM Journal on Numerical Analysis**, 55(1):144–167, 2017.

[78] P. Nagpal, N. C. Lindquist, S.-H. Oh, and D. J. Norris, *Ultrasmooth patterned metals for plasmonics and metamaterials*, **Science**, 325:594–597, 2009.

[79] D. P. Nicholls and N. Nigam, *Exact non-reflecting boundary conditions on general domains*, **J. Comput. Phys.**, 194(1):278–303, 2004.

[80] D. P. Nicholls and F. Reitich, *A new approach to analyticity of Dirichlet-Neumann operators*, **Proc. Roy. Soc. Edinburgh Sect. A**, 131(6):1411–1433, 2001.

[81] D. P. Nicholls and F. Reitich, *Stability of high-order perturbative methods for the computation of Dirichlet-Neumann operators*, **J. Comput. Phys.**, 170(1):276–298, 2001.

[82] D. P. Nicholls and F. Reitich, *Analytic continuation of Dirichlet-Neumann operators*, **Numer. Math.**, 94(1):107–146, 2003.

[83] D. P. Nicholls and F. Reitich, *Shape deformations in rough surface scattering: Cancellations, conditioning, and convergence*, **J. Opt. Soc. Am. A**, 21(4):590–605, 2004.

[84] D. P. Nicholls and F. Reitich, *Shape deformations in rough surface scattering: Improved algorithms*, **J. Opt. Soc. Am. A**, 21(4):606–621, 2004.

[85] D. P. Nicholls and F. Reitich *Boundary perturbation methods for high-frequency acoustic scattering: Shallow periodic gratings*, **J. Acoust. Soc. Amer.**, 123(5):2531–2541, 2008.

[86] D. P. Nicholls and J. Shen, *A stable, high-order method for two-dimensional bounded-obstacle scattering*, **SIAM J. Sci. Comput.**, 28(4):1398-1419, 2006.

[87] D. P. Nicholls and J. Shen, *A rigorous numerical analysis of the transformed field expansion method*, **SIAM Journal on Numerical Analysis**, 47(4):2708-2734, 2009.

[88] D. P. Nicholls and M. Taber, *Joint analyticity and analytic continuation for Dirichlet-Neumann operators on doubly perturbed domains*, **J. Math. Fluid Mech.**, 10(2):238–271, 2008.

[89] D. P. Nicholls and M. Taber *Detection of ocean bathymetry from surface wave measurements*, **Euro. J. Mech. B/Fluids**, 28(2):224–233, 2009.

[90] D. P. Nicholls and V. Tammali, *A high-order perturbation of surfaces (HOPS) approach to Fokas integral equations: Vector electromagnetic scattering by periodic crossed gratings*, **Applied Numerical Methods**, 101:1–17, 2016.

[91] Jorge Nocedal and Stephen J. Wright, *Numerical optimization*, **Springer Series in Operations Research and Financial Engineering**, Springer, New York, second edition, 2006.

[92] R. Petit, editor, *Electromagnetic theory of gratings*, **Springer-Verlag**, Berlin, 1980.

[93] H. Raether, *Surface plasmons on smooth and rough surfaces and on gratings*, **Springer**, Berlin, 1988.

[94] Lord Rayleigh, *On the dynamical theory of gratings*, **Proc. Roy. Soc. London**, A79:399–416, 1907.

[95] S. O. Rice, *Reflection of electromagnetic waves from slightly rough surfaces*, **Comm. Pure Appl. Math.**, 4:351–378, 1951.

[96] F. Reitich and K. Tamma, *State-of-the-art, trends, and directions in computational electromagnetics*, **CMES Comput. Model. Eng. Sci.**, 5(4):287–294, 2004.

[97] Jie Shen, Tao Tang, and Li-LianWang, *Spectral methods*, **volume 41 of Springer Series in Computational Mathematics**. Springer, Heidelberg, 2011. Algorithms, analysis and applications.

[98] H. Xu, E. Bjerneld, M. Käll, and L. Börjesson, *Spectroscopy of single hemoglobin molecules by surface enhanced raman scattering*, **Phys. Rev. Lett.**,83:4357–4360, 1999.

[99] Pochi Yeh, *Optical waves in layered media*, **volume 61. Wiley-Interscience**,2005.

[100] J. Zheng, J. Cheng, P. Li, and S. Lu, *Periodic surface identification with phase or phaseless near-field data*, **Inverse Problems**, page 115004, 2017.

[101] Ruixue Zhao and Jinyan Fan, *On a New Updating Rule of the Levenberg-Marquardt Parameter*, **J. Sci. Comput.**, 74(2):1146–1162, 2018.

Vita

NAME:	Matthew Christopher Kaplan
CONTACT INFORMATION:	1726 W. Carmen Ave # 3F Chicago, IL 60640 916 - 693 - 0677 matthew.c.kaplan@gmail.com
EDUCATION:	B.S., Pure Mathematics, University of Texas at Austin, Austin, 2012 M.S., Mathematics, University of Illinois Chicago, Chicago, 2014 Ph.D., Mathematics, University of Illinios, Chicago, 2018
PROFESSIONAL EXPERIENCE:	*Data Scientist* USAA Chief Technology & Digital Office, 2018 - present Member of the Chief Technology and Digital Office Data Science team. *Decision Science Intern* USAA Chief Technology & Digital Office, summer 2017 Developed forecasting models using ARIMA, CHAID, and Gradient Boosting methodologies to anticipate member behavior. *Decision Science Intern* USAA Chief Financial Office, summer 2016 Performed supervised and unsupervised cluster analyses to assist in the development of a suite of general use statistical models at the enterprise level. *Decision Science Intern* USAA Chief Financial Office, summer 2015 Collaborated with business partners to analyze customer call data and quantify the effectiveness of marketing campaign pilot programs.
TEACHING EXPERIENCE:	*Instructor and TA* University of Illinois Chicago, Department of Mathematics, Statistics, and Computer Science, 2012-2018 *Instructor and Curriculum Developer* Math Circles of Chicago, 2013-2018
PUBLICATIONS:	M. Kaplan and D. P. Nicholls, "A Nonlinear Least Squares Framework for Periodic Grating Identification with a High-Order Perturbation of Surfaces Implementation" (submitted)
HONORS:	Teaching Assistant Departmental Teaching Award, UIC, Department of Mathematics, Statistics, and Computer Science, 2017